Towards a mechanistic understanding of nanoparticle behavior using zebrafish

Arias Alpizar, G.

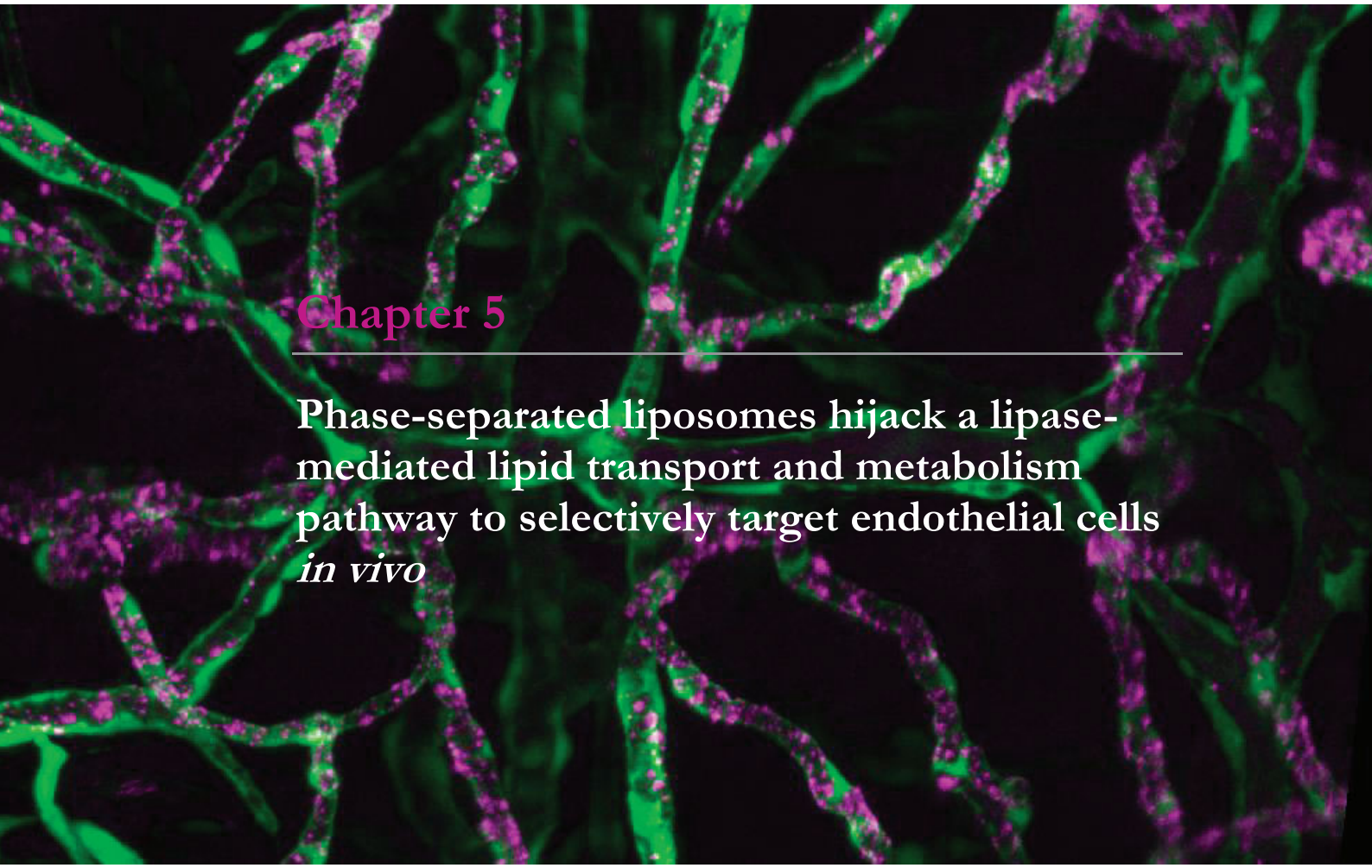

Chapter 5

Phase-separated liposomes hijack a lipase-mediated lipid transport and metabolism pathway to selectively target endothelial cells *in vivo*

Manuscript in preparation:

Arias-Alpizar, G.*; Papadopoulou, P.*; Rios, X.; Moradi, M.A.; Pattipeiluhu, R.; Bussmann, J.; Sommerdijk, N.; Llop, J.; , J.; Kros, A.; Campbell, F. Phase-Separated, "Parachute" Liposomes Hijack a Triglyceride Lipase-Mediated Lipid Transport and Metabolism Pathway to Selectively Target Endothelial Cells *in vivo*.

These authors contributed equally*

Image: Brain vasculature of a zebrafish larvae showing accumulation of PAP3 liposomes.

5.1 Abstract

Plasma lipid transport and metabolism are fundamental to ensure correct cellular function(s) throughout the body. Dynamically regulated in both time and space, the well characterized mechanisms underpinning lipid transport and metabolism offer an enticing rationale towards designing nanoparticles capable of cell selective targeting. Here, we describe a liposome formulation, composed of just two lipids, that hijacks an endogenous triglyceride lipase-mediated pathway of plasma lipid transport and metabolism to selectively target, and be taken up by, endothelial cells *in vivo*. Discovered, screened and mechanistically probed in embryonic zebrafish, liposome targeting of endothelial cells is mediated exclusively through a unique, phase-separated 'parachute' morphology. This morphology drives preferential liposome recognition and binding to endothelium-bound (endothelial) lipase. Once bound, liposomes are subsequently taken up by endothelial cells. Within the zebrafish larvae, endothelial lipase selectivity leads to liposome accumulation and intracellular uptake at the brain endothelium. In young mice, extensive liposome accumulation within the liver and spleen matches the high expression of endothelial lipase within these metabolic organs. Overall, these compositionally simplistic liposomes offer new avenues towards the discovery of lipid-based nanoparticles capable of cell selective targeting *in vivo*.

5.2 Introduction

All cells rely on plasma lipid transport to maintain the correct intracellular balance of essential and non-essential fatty acids. This requires dynamic regulation of the secretion, transport, and metabolism of water-insoluble fats throughout the body. Often packaged as nanometer-sized, solid lipid particles (*i.e.* lipoproteins), many of the biological mechanisms regulating plasma lipid transport and metabolism are well understood[1] and provide an enticing rationale to design lipid-based nanomedicines capable of preferential cellular targeting. To date however, Onpattro® - a lipid nanoparticle (LNP)-based RNAi therapy - remains the only example of a lipid-based nanomedicine explicitly functioning through hijacking of an endogenous plasma lipid transport and metabolism pathway (*i.e.* apolipoprotein E-mediated targeting of the low density lipoprotein receptor (LDLR)) to preferentially target specific cells (*i.e.* hepatocytes) of the body.[2, 3]

The three main plasma lipid transport forms are free fatty acids (FAs), triglycerides (TGs) and cholesteryl esters (CEs).[1] Free FAs are generally transported as a complex with serum albumin, whereas TGs and CEs are transported within the core of plasma lipoproteins – solid lipid particles surrounded by a lipid monolayer rich in phospholipids and stabilized by apolipoprotein(s). The five major classes of lipoproteins are chylomicrons, very low density lipoproteins (VLDLs), intermediate density lipoproteins (IDLs), low density lipoproteins (LDLs) and high density lipoproteins (HDLs). Dietary fats (*i.e.* essential fatty acids) are processed within the intestine and secreted into blood as chylomicrons (*guide size*: 100 – 1000 nm); endogenous fatty acids are primarily processed within the liver and secreted as VLDLs (*size*: 50 - 200 nm); IDLs and LDLs (*size*: 20 - 50 nm) are lipoprotein metabolites enriched in cholesterol and, at high levels, are associated with atherogenic disorders;[4, 5] and HDL (*size:* 8-12 nm) is primarily involved in cholesterol reverse transport, sequestering excess cholesterol from lipoproteins and/or cells and transporting it back to the liver.[6] With the exception of HDL, a single, surface-bound apolipoprotein B (apoB100 or apoB48 for VLDL and chylomicrons respectively) stabilizes each secreted lipoprotein. HDLs, in contrast, are stabilized by apolipoprotein A-I (apoAI).[7, 8]

Once secreted into the bloodstream, soluble and exchangeable apolipoproteins (*e.g.* apoA, C, D and E) recognize and bind to the surface of a circulating lipoprotein. Binding preference is modulated by lipoprotein size (*i.e.* curvature),

composition and local/systemic apolipoprotein concentrations. Once bound, apolipoproteins guide lipoproteins to specific targets within the body. For example, apoE is a ligand for LDLr, promoting uptake primarily in hepatocytes;[9] apoA1 is a cofactor of lecithin cholesterol acyltransferase (LCAT),[10] promoting the conversion of cholesterol to cholesteryl esters; and lipoprotein-bound apoC2 functions as an obligatory cofactor of lipoprotein lipase (LPL).[11, 12]

Following transport, lipoproteins are typically metabolized to release extracellular free fatty acids at the target site that are subsequently taken up by cells locally. For this, triglyceride lipases are key hydrolytic enzymes that regulate lipid metabolism throughout the body. The three principle members of the triglyceride lipase family are LPL,[13] hepatic lipase (HL),[14] and endothelial lipase (EL)[15, 16] (encoded by the human genes *LPL*, *LIPC,* and *LIPG* respectively). All three share significant structural homology, including a conserved catalytic triad of amino acids (serine, aspartate and histidine), as well as conserved heparin and lipoprotein binding domains.[15, 16] LPL is mainly synthesized in adipose tissue, heart and skeletal muscle, HL in hepatocytes, and EL in vascular endothelial cells.[15] Once expressed, triglyceride lipases are secreted and actively transported (in the case of LPL and HL) to the local endothelium where they anchor to heparan sulfate proteoglycans (HSPG) *via* electrostatic interactions.[17] As hydrolytic enzymes, LPL primarily hydrolyzes triglycerides,[18] HL – triglycerides and phospholipids,[14, 19] and EL – phospholipids.[15] Substrate specificity is determined by sequence variation in the lid region of each enzyme.[15, 20, 21] However, whereas LPL and HL metabolize fats primarily derived from VLDL and chylomicrons, the principle function of EL is the regulation of HDL metabolism *via* interactions with apoA-1. [15, 22-25] In addition, all three triglyceride lipase family members are capable of internalizing lipoproteins *via* proteoglycan- or receptor-mediated pathways in a non-enzymatic fashion.[17, 26]

Herein, we describe an intravenously (*i.v.*) administered liposome formulation, composed of just two lipids, that selectively targets endothelial cells *via* an endogenous triglyceride lipase-mediated mechanism of recognition, binding, and intracellular uptake. With no additional functionality, liposome targeting selectivity is exclusively mediated through a phase-separated, “parachute” morphology. Our data strongly suggests a targeting preference for EL over other triglyceride lipases, however, given their promiscuous function and close structural homology, contributions from other lipases cannot be excluded. Within embryonic zebrafish, liposomes selectively target, and are taken up by, brain endothelial cells (bECs). Within 6-8 week old mice, liposomes predominantly accumulate within the liver and spleen. Specific targeting

strategies of triglyceride lipase-mediated mechanisms become attractive due to the importance of EL in cardiovascular disease and its overexpression in different tumors. This work contributes to the preferential targeting of triglycerides lipase mediated mechanisms and shed the light on the design of new nanotechnology platforms based on endogenous mechanisms of plasma lipid transport and metabolism.

5.3 Results

PAP3 liposomes accumulate at the brain endothelium of embryonic zebrafish

Zebrafish embryos are convenient, accurate and cost effective animals to study the behavior and pharmacokinetics of nanoparticles *in vivo*,[27, 28] to assess and predict key nanoparticle-liver interactions within higher vertebrates[29, 30] and to identify the biological mechanisms underpinning nanoparticle fate *in vivo*.[29-31] From a preliminary screen of *i.v.* administered liposomes, we unexpectedly observed selective accumulation of a liposomal formulation, PAP3, within the head region of a three-day old (~78 hpf) zebrafish embryo (**Figure 1a,b**). PAP3 liposomes (size: ~120 nm) were composed of an equimolar mixture of just two lipids, a novel synthetic lipid, 2-hydroxy-3-oleamidopropyl oleate (DOaG), and naturally occurring, 1,2-distearyl-*sn*-glycero-3-phosphocholine (DSPC) (**Figure 1c**). These liposomes contained no additional targeting functionality. Looking closely within the head region of the zebrafish embryo, PAP3 liposomes clearly accumulated within some (*e.g.* mesencephalic vein (MsV), mesencephalic artery (MsA), middle mesencephalic central artery (MMCtA), middle cerebral vein (MCeV), primordial hindbrain channels (PHBC) and cerebral arteries (CtAs)), but not all (*e.g.* dorsal longitudinal vein (DLV), primordial midbrain channel (PMBC)) blood vessels and capillaries (**Figure 1d**). These specific blood vessels and capillaries in which PAP3 liposomes selectively accumulated have been previously characterized as the brain endothelium (*i.e.* bECs), constituting the blood-brain-barrier (BBB) of the developing embryo.[32-34]

In terms of a neurovascular unit, anatomical features that regulate mammalian brain homeostasis and permeability are conserved in zebrafish. These features include endothelial tight junctions, maintained by specialized tight junction proteins (*e.g.* Claudin-5);[33, 35, 36] pericytes and glia cells surrounding the brain vasculature;[37, 38] and the expression of substrate specific transporters (*e.g.* GLUT1).[39] All these features are present and functional (as assessed by

permeability assay) within the embryonic zebrafish by 3 days post-fertilization (dpf).[40] Importantly, angiogenesis within the brain of the embryonic zebrafish is temporally coupled to barriergenesis.[39] This means nascent bECs immediately express genes associated with BBB function. As such, the dynamic expression of the tight junction protein Claudin-5, encoded by *claudin5a*, has been used to dynamically map the developing brain endothelium of the embryonic zebrafish over time.[33, 35, 36, 39] This simple and clear delineation of brain versus systemic endothelial cells within the head region of the embryonic zebrafish provides an ideal *in vivo* screening platform to assess potential bEC targeting specificity of nanoparticles using standard fluorescence microscopy setups (**Figure 2a** and **Supplementary Figure 1a**).[33,35, 36]

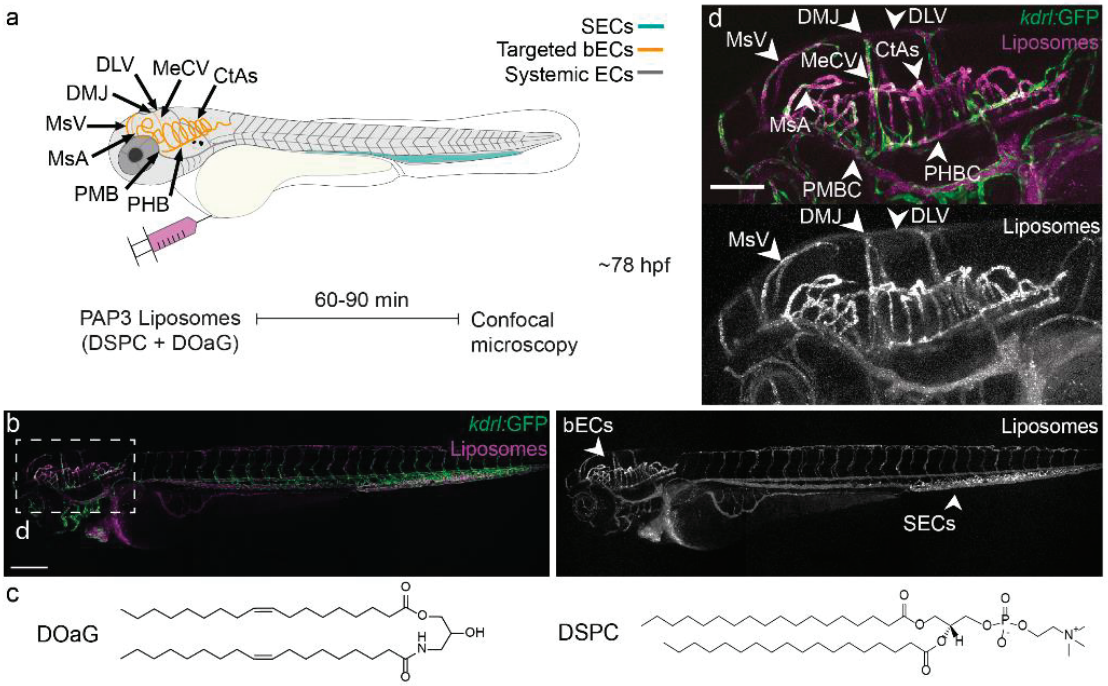

Figure 1. Biodistribution of PAP3 liposomes in zebrafish larvae. (a) Schematic zebrafish larvae in lateral (whole body) view, showing the site of microinjection and key cranial vessels. Fluorescently labeled liposomes are imaged with confocal microscope after 60-90 min. The vasculature as follows, liposomes targeted bECs in yellow and systemic endothelium in dark gray, scavenging endothelial cells (SECs) in cyan, at ~72 hours post fertilization (hpf). **(b)** Biodistribution of PAP3 liposomes (magenta/grey) in Tg(*kdrl*:GPF), expressing GFP in all endothelial cells, lateral view (10x magnification) at 78 hpf, 1.5 hours post injection (hpi). **(c)** Chemical structure of lipids used in equimolar mixture for the formulation of PAP3 liposomes, DOaG and DSPC lipids. **(d)** Zoom of the cranial region in lateral view. bECs, brain endothelial cells; CtAs, central arteries; DLV, dorsal longitudinal vein; DMJ, dorsal midline junction; MCeV, middle cerebral vein; MsA, mesencephalic artery; MsV, mesencephalic vein; PMBC, primordial midbrain channel; PHBC, primordial hindbrain channel; SECs, scavenging endothelial cells. Liposomes prepared by extrusion, concentration 5 mM containing 0.2 mol% DOPE-LR. Scale bars: 200 µm (lateral view) and 100 µm (zoom).

To verify selective accumulation with bECs, PAP3 liposomes were administered (*i.v.*) within embryonic zebrafish at different developmental stages (2, 3 and 4 dpf) (**Figure 2b-d**). This two-day timeframe spans the late-stage development of the embryonic BBB, most prominently within the mid- and forebrain, following complete hindbrain vascular invasion by 48 hpf (characterized by CtA capillary loops connecting both PHBCs with the central basilar artery (BA)).[32] Accordingly, at 2 dpf, PAP3 liposomes mainly targeted functional bECs within blood vessels and capillaries of the hindbrain, namely CtAs, BA and PHBCs (**Figure 2b**). At 3 dpf, as blood vessels irrigate rostrally throughout the brain,[41] PAP3 liposomes accumulated within newly formed capillaries of the mid- and forebrain (**Figure 2e**), as well as within the continually expanding BBB vasculature of the hindbrain (**Figure 2f-h** and **Supplementary Figure 1a-b** for a Z-stack depth color-coded of the vasculature in dorsal view). At 4 dpf, PAP3 liposomes extensively accumulated throughout the now developed brain endothelium of the embryonic zebrafish (**Figure 2d**)**.** Notably at all developmental stages, liposomes remained freely circulating within systemic blood vessels (*e.g.* PMBC and DLV) (**Figure 2i**)**,** confirming a targeting preference of PAP3 liposomes for bECs. Indeed, colocalization of PAP3 liposome accumulation and Claudin-5 expression, notably within the CtAs, MMCtA (**Figure 2h-i**) and MsA, was confirmed in Tg*(cldn5a:*eGFP*)*[33] embryos stably expressing an integrated eGFP-Claudin5a fusion protein (**Figure 2j-k** and **Supplementary Figure 1c**)**.**

In addition to bEC targeting, PAP3 liposomes also accumulated within the caudal hematopoietic tissue (CHT) and caudal vein (CV) of the embryo (**Fig. 1a,b**)**.** We have previously shown that these blood vessels are composed of scavenger endothelial cells (SECs) that are genetically and functionally equivalent to liver sinusoidal endothelial cells (LSECs) in mammals.[29] These cells proficiently clear anionic (as well as 100% DSPC liposomes) nanoparticles from circulation, predominantly mediated by the scavenger receptors, Stabilin-1 and -2. Administration of PAP3 liposomes in zebrafish mutants lacking scavenger receptors Stabilin-1 and Stabilin-2 (*stabilin-1*^{ibl3} *stabilin-2*^{ibl1})[30] (**Supplementary Figure 2**) resulted in significantly reduced liposome accumulation within the CHT and CV of the embryo whilst maintaining bEC targeting. This confirmed that (off-)targeting of PAP3 liposomes to SECs but not bECs was Stabilin-dependent.

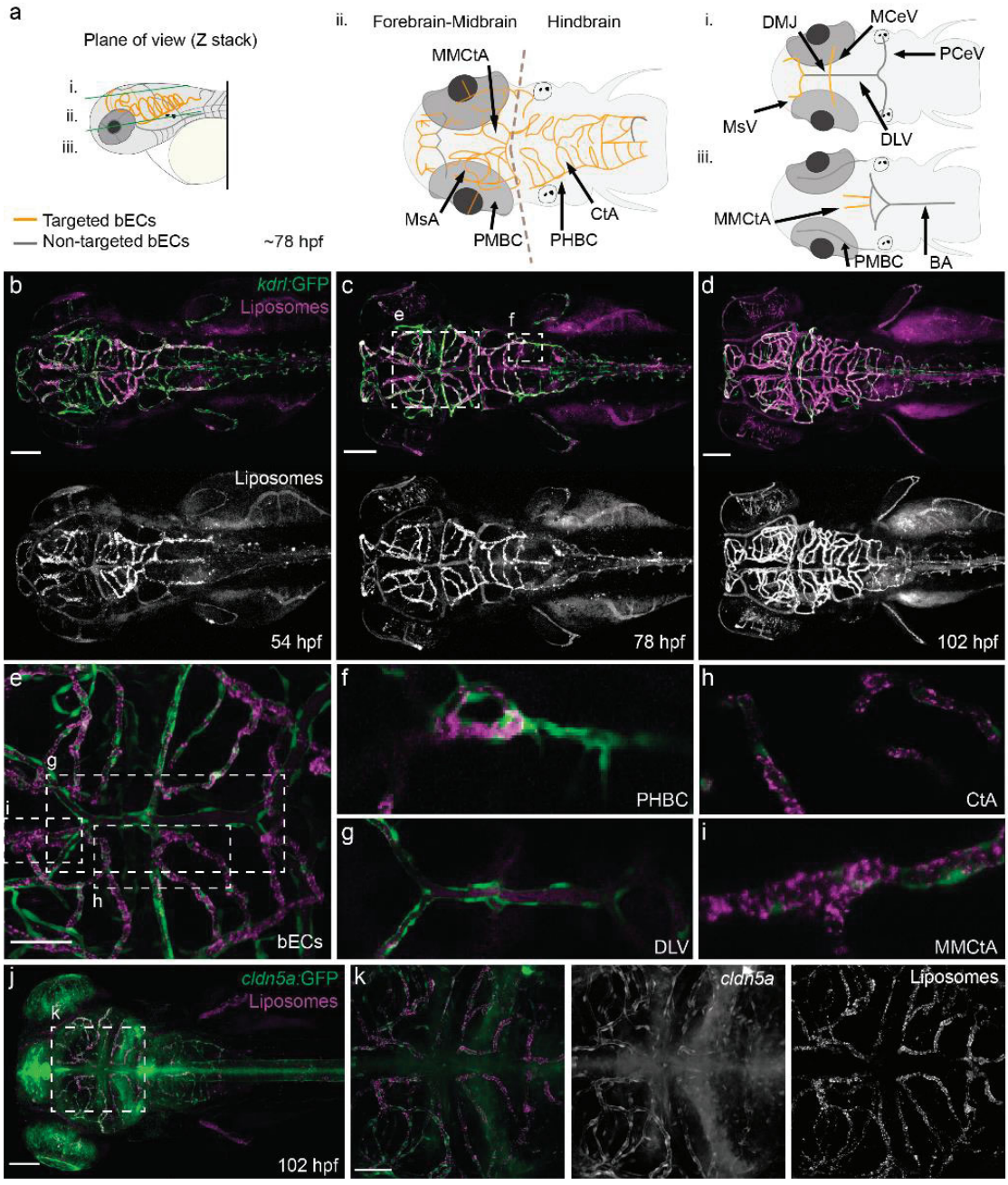

Figure 2. PAP3 liposomes accumulate in the bECs of zebrafish. (a) Schematic zebrafish larvae with key blood vessels in different planes of view. See **Supplementary Figure 1a-b** for a Z-stacks depth color-coded zebrafish vasculature. Dorsal view, showing the **i.** top, **ii.** middle and **iii.** bottom layer diagram. The vasculature as follows, targeted brain endothelial cells (bECs) in yellow and non-targeted systemic endothelium in dark gray, at ~78 hours post fertilization (hpf). PHBC, primordial hindbrain channel; CtA, central artery; DLV, dorsal longitudinal vein; MsA, mesencephalic artery; MsV, mesencephalic vein; MMCtA, middle mesencephalic central artery. (**b**) Biodistribution of PAP3 liposomes (magenta/grey) in dorsal view (10x magnification) 1.5 hpi at 54 hpf, **(c)** 78 hpf, **(d)** 102 hpf. Inset of **(e)** shows the biodistribution of PAP3 liposomes in bECS. **(f)** Posterior part of the PHBC, **(g)** DLV, **(h)** CtA, **(i)** MMCtA in Tg(*kdrl:*GFP). **(j-k)**

Biodistribution of PAP3 liposomes (magenta/grey) in Tg*(cldn5a:*GFP*)* transgenic line with GFP-labeling blood and choroid plexus brain barrier showing colocalization of *cldn5a* with fluorescent liposomes. Zoom in of the region that includes the hindbrain vasculature and colocalization with *cldn5a* expression is shown in **Supplementary Figure 1c**. Liposomes prepared by extrusion, concentration 5mM containing 0.2 mol% DOPE-LR. Scale bars: 100 µm (dorsal view), 50 µm (tissue level).

CryoTEM revealed a novel 'parachute' liposome morphology that is essential for BBB targeting in embryonic zebrafish

To rationalize bEC targeting specificity, and in the absence of any additional targeting functionality (*e.g.* targeting ligands), cryogenic transmission electron was used. Unexpectedly, these images revealed a highly unusual, phase-separated "parachute" morphology, characterized by a single electron rich protrusion within each liposomal membrane (**Figure 3a-c** and **Supplementary Figure 3**)**.** Such parachute-like structures have been previously reported for vesicle-polymer hybrid nanoparticles[42, 43] but not purely lipidic nanoparticles. Given the flat, bilayer preference of amphipathic DSPC, we assume that the observed phase-separated protrusion is rich in PAP3 lipid. Indeed, at a molecular level, DOaG is structurally very similar to a diacylglycerol (DAG) whose hydrophobicity and geometry are known to decrease the spontaneous curvature of PC lipid membranes and perturb lamellar membrane structures resulting in the formation of non-bilayer phases.[44-48]

To correlate phase separation and bEC targeting, PAP3 liposomes were formulated at varying molar ratios (10-50 mol% DOaG; >50 mol% DOaG resulted in severe liposome aggregation) and both liposome morphology and *in vivo* (zebrafish larvae) biodistribution were compared (**Figure 3d-i**). As reference, pure DSPC liposomes were characteristically non-spherical, bi-layered particles and were proficiently cleared by SECs (within the CHT and CV) of a three day old zebrafish embryo (**Supplementary Figure 4**). This biodistribution mirrored that of DSPC liposomes in a two day old zebrafish embryo whose uptake within SECs was shown to be Stabilin mediated.[29] CryoTEM images of PAP3 liposomes (10 mol% DOaG) revealed a mixture of non-spherical, bi-layered or multilamellar particles with no evident phase separation (**Figure 3d, Supplementary Figure 5a**). As for DSPC liposomes, these liposomes mostly accumulated with SECs within the CV and CHT of the larvae (**Supplementary Figure 6a**) and did not target bECs (**Figure 3e**). Likewise, PAP3 liposomes (20 mol% DOaG) were predominantly non-spherical (**Figure 3f, Supplementary Figure 5b**), mainly accumulated within SECs (**Supplementary Figure 6b**) and

did not target bECs (**Figure 3g**). However, in this case, small electron-rich protrusions within the liposome membrane suggested a liposome formulation approaching its miscibility threshold (**Figure 3f –** white arrows). This was confirmed by the phase separation of PAP3 (30 mol%) liposomes whereby a single lipid protrusion was now clearly associated with each discreet liposome (**Figure 3h, Supplementary Figure 5c**).

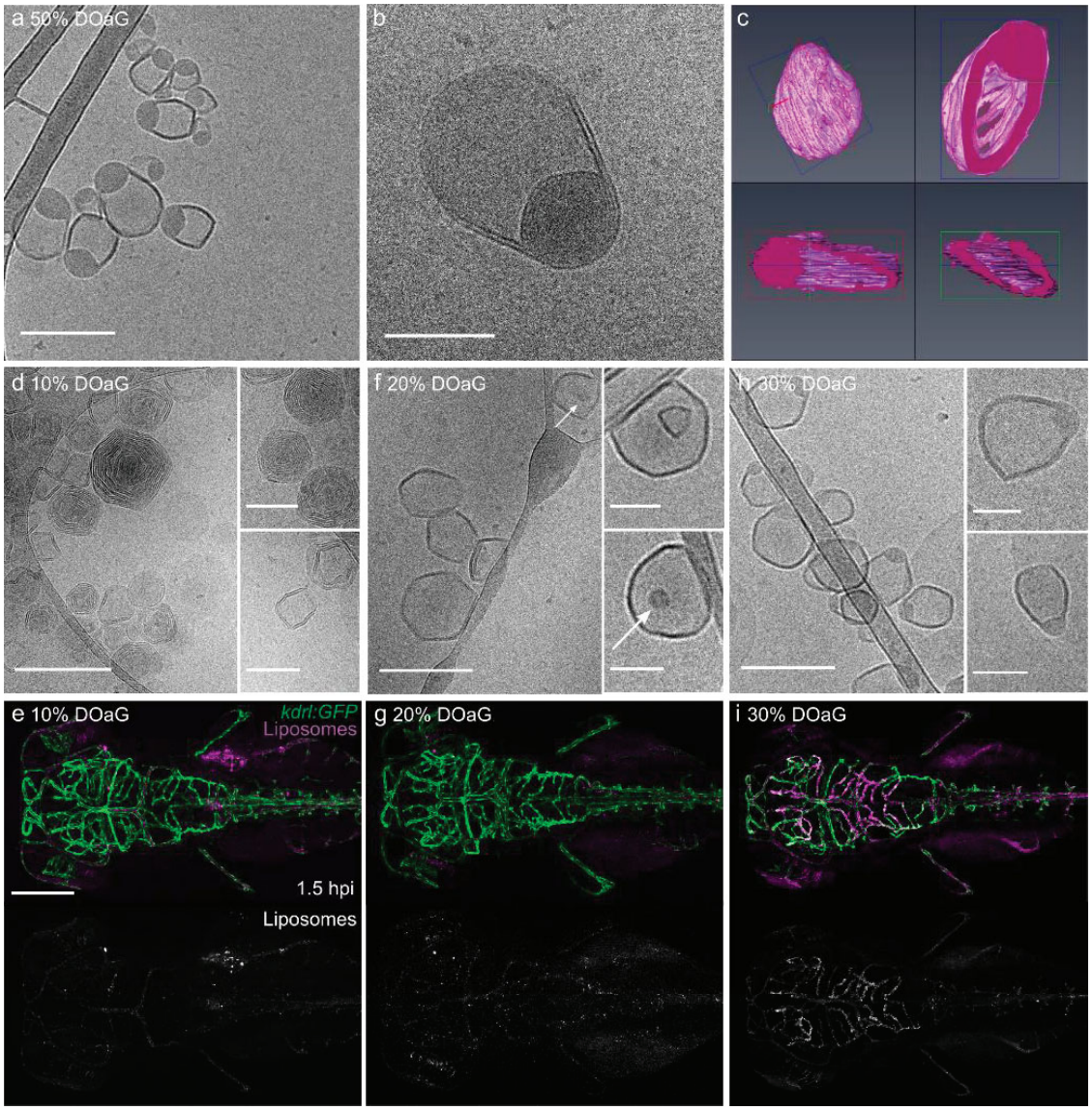

Figure 3. CryoTEM of PAP3 liposomes characterized by phase separation correlates with the bECs targeting in zebrafish larvae. (a-b) CryoTEM of PAP3 (50 mol% DOaG) liposomes and **(c)** Tomography of a representative PAP3 (50 mol% DOaG) liposome from different angles**.** Cryo-TEM and biodistribution (magenta/grey) of **(d-e**) DOaG 10 mol%, **(f-g)** 20 mol%, and **(h-i)** 30 mol%. Biodistribution in Tg*(kdrl:*GFP*)* at ~78 hpf, 1.5 hpi, liposomes concentration 5 mM containing 0.2 mol% DOPE-LR. Liposomes described in all panels made by ethanol injection except panel **b** and **c**, made by extrusion. Scale bars: 200 nm and 100 nm for higher magnification insets for CryoTEM and 200 µm for dorsal view.

PAP3 (30 mol% DOaG) liposomes, as for PAP3 liposomes (*i.e.* 50 mol% DOaG), proficiently targeted bECs of the zebrafish larvae (**Figure 3i** and **Supplementary Figure 6c**). The miscibility threshold of approximately 30 mol% DOaG (within a DSPC bilayer) closely mirrored the value previously reported for structurally similar DAG (25 mol% miscibility threshold) within a PC bilayer.[49] Accordingly, replacing PAP3 with its diacylglycerol analogue 1,3-dioleyolglycerol (DOG) (**Supplementary Figure 7a**), also resulted in phase-separated liposomes and bEC targeting (**Supplementary Figure 7b-d**). Phase separation is also dependent on the gel phase state of a lipid bilayer. Consequently, switching co-formulant phospholipid from saturated DSPC (phase transition temperature (T*m*) 55°C) to unsaturated DOPC (T*m* -17°C) resulted in liposomes (at room temperature) with no apparent phase separation and severely ablated bEC targeting (**Supplementary Figure 8**). Altogether, these experiments confirmed the critical requirement of phase-separated lipid protrusions for bEC selective liposome accumulation within the embryonic zebrafish.

PAP3 liposome targeting and uptake by bECs in zebrafish larvae is mediated by (endothelial) lipase

In the absence of any additional targeting functionality (*i.e.* targeting ligands), we next investigated whether PAP3 liposomes could be hijacking endogenous plasma lipid transport mechanisms to selectively target bECs of the embryonic zebrafish. Importantly, all major elements of mammalian plasma lipid transport and metabolism, including the expression of apolipoproteins, lipoprotein receptors (*e.g.* low density lipoprotein receptor, LDLR) and enzymes (*e.g.* lipases), are present and functional in a three day old zebrafish embryo.[50-52] These conserved features have led to the zebrafish being widely used as *in vivo* model to investigate various lipid disorders,[53-55] including hypertriglyceridemia, a disease caused by a malfunction in lipase-mediated plasma lipid transport and metabolism.[56]

Following secretion into blood, the typical first step of lipoprotein-mediated plasma lipid transport is the binding of soluble apolipoproteins.[1] To identify serum proteins preferentially adsorbed to PAP3 liposomes, we therefore first performed a photoaffinity-based capture of the liposome protein corona.[57] Importantly, given the practical difficulties in obtaining sufficient embryonic zebrafish serum, these experiments were performed in human serum and do not necessarily reflect the exact composition and abundance of serum proteins in the developing zebrafish embryo. For this method, it was necessary to incorporate

the photoaffinity probe, IKS02 (5 mol%),[57] within the PAP3 liposome formulation. Incorporation of this probe did not significantly alter the physicochemical properties or *in vivo* behavior of PAP3 liposomes (**Supplementary Table 1**). Following protein corona capture, isolation, and subsequent proteomic analysis, we identified soluble apolipoproteins as the major protein corona components of both PAP3 and control DSPC liposomes (**Supplementary Figure 9**). However, no obvious differences in protein corona composition could easily explain the very different *in vivo* fates of these two liposome formulations. In contrast, when compared to the characterized protein corona of near-neutral liposomes based on the lipid composition of Myocet®,[57] the significant enrichment of apoA1 and A4, as well as the presence of apoC2 and C3, on the surface of PAP3 liposomes, at least conformed to a lipoprotein-like transport and metabolism targeting rationale.

Given the presence of apolipoproteins on the surface of PAP3 liposomes, we next investigated the potential role of lipases in the selective recognition and binding of PAP3 liposomes within the embryonic fish. Lipases are heparin-releasable[14, 58] and following heparin pre-injection (*i.v.*; 30 minutes prior to PAP3 liposome administration), PAP3 liposomes predominantly remained in circulation with no apparent bEC targeting (**Figure 4a-f**). While this strongly suggested lipase involvement, heparin is also known to bind a wide range of other proteins that could (in)directly disrupt liposome targeting of bECs.[59] To confirm lipase-mediated recognition, we therefore inhibited lipase activity within the embryonic fish using the selective lipase inhibitor, XEN445.[60, 61] This resulted in a significant decrease in bEC targeting of PAP3 liposomes and confirmed triglyceride lipases play a fundamental role in PAP3 liposome targeting selectivity within the embryonic fish (**Figure 4g-i**). Furthermore, XEN445 has demonstrated high selectivity for EL (IC_{50} = 237 nM) over LPL (IC_{50} = 20 μM) and HL (IC_{50} = 9.5 μM).[60] Taken together with the high expression of EL within the head region of zebrafish embryos[62] (from 2 to 4 dpf) and the observed dominance of apoA1 on the PAP3 liposome surface, it is plausible that PAP3 liposomes preferentially target EL by hijacking endogenous mechanisms of HDL recognition and metabolism.[15, 23] Given the promiscuous and overlapping functions of the triglyceride lipase family members, however, it is not possible to exclude contributions of other triglyceride lipase family members.

Completing its journey within the embryonic zebrafish, we finally assessed the fate of PAP3 liposomes following (endothelial) lipase-mediated recognition and binding at the luminal surface of bECs. Surprisingly, we observed that liposomes already associated with bECs were no longer heparin-releasable (**Figure 5a-c**).

This suggested PAP3 liposomes, following initial lipase-mediated attachment, were processed by bECs and internalized *via* non-enzymatic mechanisms of lipase-mediated lipoprotein. As stated previously, lipase-mediated lipoprotein internalization is particular proficient in the case of EL-mediated uptake of HDL particles.[17, 26] To investigate potential intracellular uptake of PAP3 liposomes, the endosomal pH-sensitive dye, pHrodo™, was incorporated within the PAP3 liposome membrane *via* a phospholipid anchor (as in reference [28]) (**see Supporting Information** for characterization and **Supplementary Figure 10** for pH-dependent emission). Incorporation of this fluorescent probe did not significantly alter the size or bEC targeting proficiency of PAP3 liposomes (**Supplementary Table 1**).

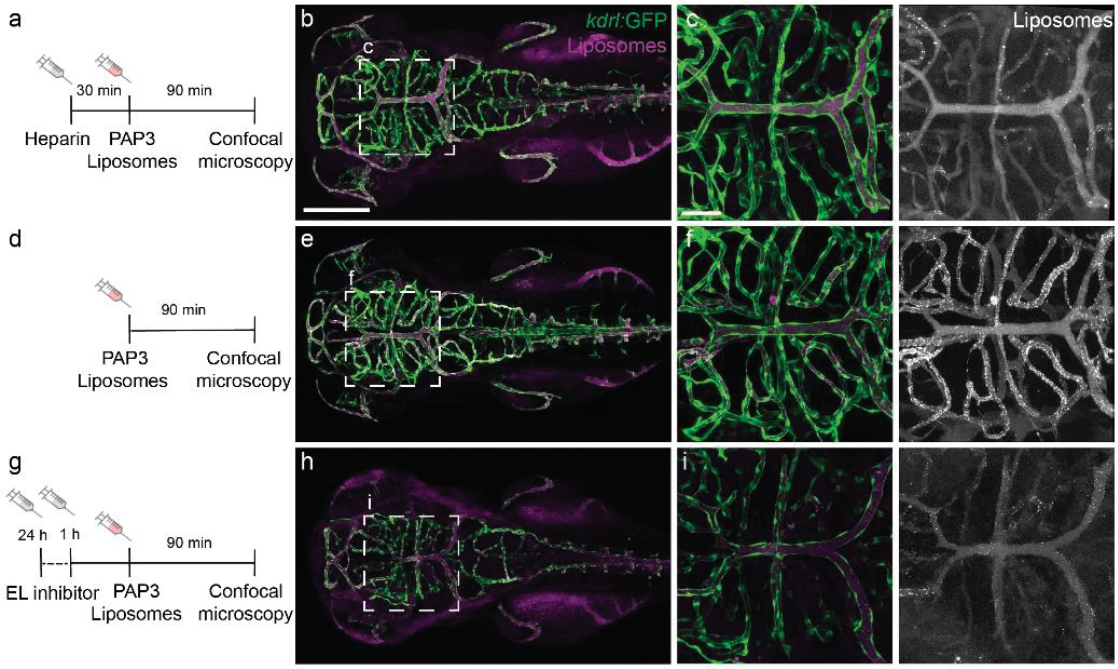

Figure 4. bECs targeting by PAP3 liposomes is inhibited by heparin and an EL lipase inhibitor. (a) Timeline of injection and imaging. **(b-c)** Biodistribution of PAP3 liposomes (in magenta or grey) (10 and 40x magnification) after heparin administration, **(d)** Timeline (injection and imaging). **(e-f)** Biodistribution of PAP3 liposomes at 1.5 hpi. **(g)** Timeline. **(h-i)** Biodistribution of liposomes (1.5 hpi) after a double (24 h and 1 h prior liposomes) administration of an EL inhibitor (XEN 445,1 nl of 50 mM). All zebrafish larvae, Tg*(kdrl:*GFP*)* at ~78 hpi. Liposomes made by extrusion, concentration 5 mM containing 0.2 mol% DOPE-LR. Scale bars: 200 µm (whole embryo) and 50 µm (tissue level).

Following liposome administration, pHrodo™-associated fluorescence was clearly observed within the brain endothelium, *e.g.* CtAs and MMCtA, but not systemic blood vessels, *e.g.* DLV or PMBC (**Figure 5e-f**).This mirrored the observed biodistribution of PAP3 liposomes and suggests PAP3 liposomes are endocytosed by bECs following initial lipase-mediated recognition and attachment.

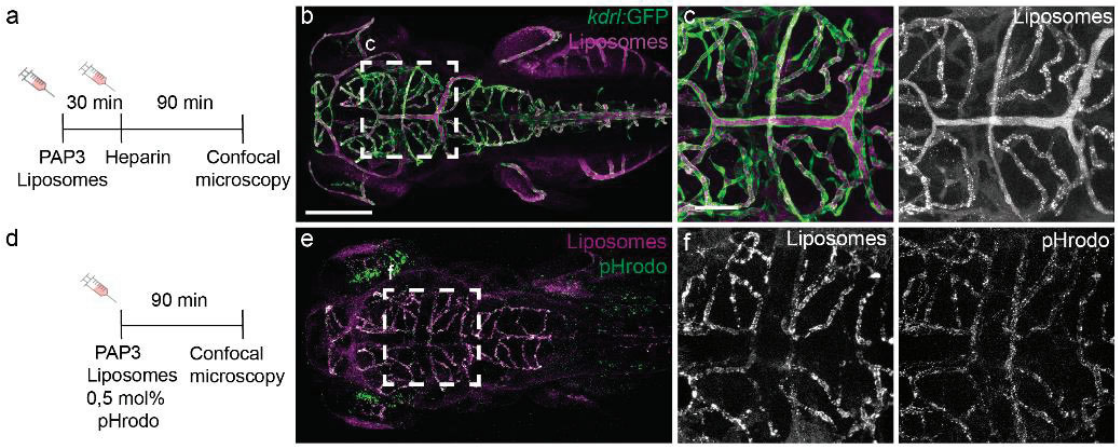

Figure 5. Internalization of PAP3 by zebrafish bECs. (a) Timeline of injection and imaging. **(b-c)** Biodistribution of PAP3 liposomes (5 mM containing 0.2 mol% LR-DOPE, in magenta of grey) (10 and 40x magnification) after post-administration of heparin. **(d)** Timeline of injection and imaging. **(e-f)** Biodistribution of PAP3 liposomes (10 mM) containing 0.5 mol% of pH sensitive DOPE-pHrodo (green/grey) to indicate endocytosis and 0.5 mol% of non-sensitive pH dye NBD (magenta/grey) to label liposomes. All zebrafish larvae at ~78 hpi. Liposomes made by extrusion. Scale bars: 200 µm (whole embryo) and 50 µm (tissue level).

PAP3 liposomes target the liver and spleen in mice

To correlate our findings in mammals, we quantified the dynamic biodistribution of PAP3 liposomes following *i.v.* administration in 6-8 week old female mice (**Figure 6a**). For these experiments, a non-exchangeable ^{64}Cu ($T_{1/2}$= 12,7 h) radionuclide was incorporated as positron emission tomography (PET) tracer. To chelate ^{64}Cu to the liposome membrane, the lipid-NOTA conjugate, NOTA-Bz-SCN-C18 (0.2 % mol), was incorporated within the PAP3 formulation. Based on 'cold' experiments using stable Cu isotopes, the incorporation of this lipid and/or Cu chelation protocol did not affect the physicochemical properties, morphology and/or bEC targeting proficiency of PAP3 liposomes in embryonic zebrafish (**Supplementary Figure 11** and **Table 1**). Following tail vein injection (930±50 kBq/100 µL; n=3), PET scans were obtained, from 1 min to 24 hours post-injection, to visualize and quantify (% injected dose per cm^3; %ID/cm^3) *in vivo*

liposome biodistribution (**Figure 6b**). Calculated *in vivo* values were subsequently validated through *ex vivo* radioanalysis (%ID/g) of major organs (heart, brain, liver, spleen, kidney, lung, and stomach) and blood, following cardiac perfusion and organ collection at selected time points (10 min, 2 h and 24 hpi) (**Figures 6c-e**). These analyses revealed rapid and extensive accumulation of PAP3 liposomes within the murine liver and spleen, with values of *ca.* 70% ID/cm^3 and 25% ID/cm^3 of the liposome injected dose accumulated in liver and spleen, respectively, at 10 min post-injection. This strongly suggested active clearance of PAP3 liposomes within these two organs. In contrast, low accumulation was observed in any other major organ analyzed and, unlike the zebrafish larvae, murine brain accumulation of PAP3 liposomes was negligible. Equivalent values were obtained in *ex vivo* experiments using gamma counting (**Figures 3d** and **3e**).

The extensive and rapid accumulation of PAP3 liposomes within the murine liver and spleen correlates with the high expression of EL within both these metabolic organs.[15, 16] However, EL is also known to be highly expressed in other organs with high metabolic rates and vascularization, notably the lungs. The absence of any significant PAP3 liposome accumulation within the lungs may, therefore, indicate a significant proportion of PAP3 liposomes are scavenged by LSECs within the liver and spleen, presumably in a Stabilin-1 and -2 dependent manner, as was observed in the zebrafish larvae (**Figure 1b**), and/or phagocytosed by Kupffer cells (*i.e.* liver resident macrophages) and splenic macrophages.

5.4 Discussion and Conclusion

Described is a liposome formulation, consisting of just two lipid reagents, that proficiently targets endothelial cells *via* an endogenous (endothelial) lipase-mediated mechanism of recognition and cellular uptake. While lipases, in particular small secretory phospholipase A_2 (sPLA2), have been previously exploited to achieve localized, stimuli-responsive drug release within target tissues (*e.g.* solid tumors),[63, 64] nanoparticle targeting HSPG-anchored triglyceride lipases, functioning as both attachment and bridging biomolecule, has not before been described.

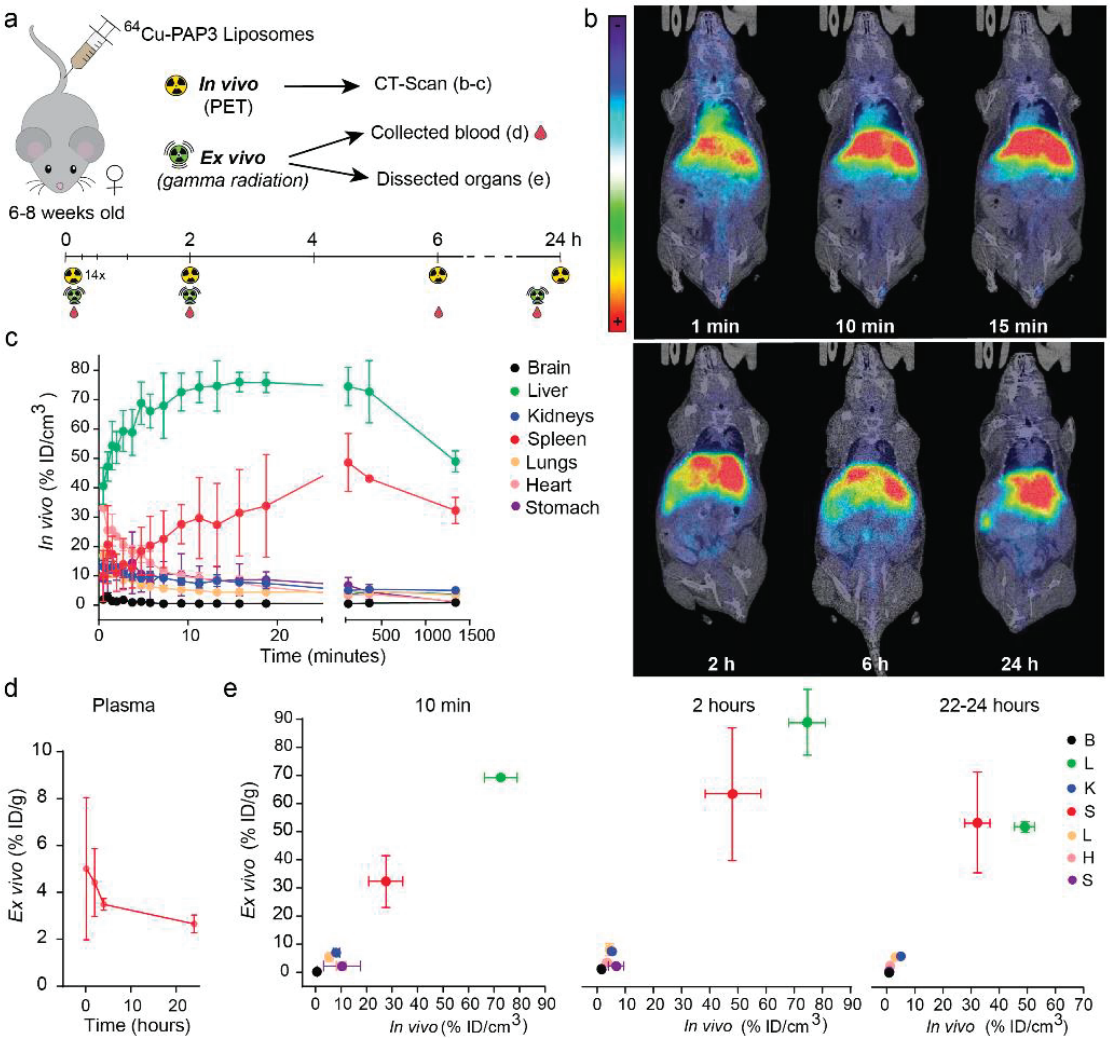

Figure 6. Biodistribution of radiolabeled PAP3 liposomes in mice. (a) Scheme of injection, PAP3 radiolabeled liposomes containing 0.2 mol% of ^{64}Cu-NOTA-Bz-SCN-C18 were injected in 6-8 weeks female mice (n=3). I*n vivo* and *ex vivo* experiments using positron emission tomography (PET) and gamma radiation counter, including blood samples, were performed at different time points (up to 24 h). **(b)** Representative PET images (coronal projections) obtained at 1, 10, 15 min and 2-6-24 h after injection of PAP3 liposomes. PET images have been co-registered with representative CT slices for anatomical localization of the radioactive signal. **(c)** *In vivo* quantitative tracer uptake values in brain, liver, kidneys, spleen, lungs, heart and stomach, at 0.5, 1, 1.5, 2.75, 3.75, 4.75, 5.75, 7.25, 9.25, 11.25, 13.25, 15.75, 18.75, 120, 360, 1340 minutes after injection. Measurements are decay-corrected and presented as %ID/cm^3. **(d)** Concentration of radioactivity in plasma at 10 min, 2, 6 and 24 h after *i.v.* administration of ^{64}Cu-labelled PAP3 liposomes. **(e)** Correlation between concentration of radioactivity in different organs (brain, liver, kidneys, spleen, lungs, heart and stomach) as determined by PET imaging (*in vivo*) and dissection/gamma counting (*ex vivo*) at 10min, 2 and 22-24 h after administration.

Lacking any additional targeting functionality, lipase recognition of PAP3 liposomes is exclusively mediated through a unique 'parachute' morphology, characterized by a single, phase-separated lipid protrusion. This protrusion resembles, in both structure and size, a solid lipid nanoparticle (*i.e* lipoprotein), and, as for analogous DAG/PC lipid mixtures, is likely characterized by increased stress on a bended membrane and increased surface hydrophobicity.[65, 66] Importantly, however, although stable in ddH_2O, PAP3 liposomes formulated in physiological salt solution (and in the absence of serum proteins) were highly unstable. As for endogenous lipoproteins (requiring apoB-48, apoB-100 or apoA-I for chylomicrons, VLDL and HDL, respectively),[1] PAP3 liposome serum stability therefore appears to be dependent on the adsorption of soluble apolipoproteins (*e,g.* apoA1) to the liposome surface. While greater molecular understanding of how these phase-separated protrusions are incorporated within the PAP3 liposome membrane is undoubtedly needed, the compositional simplicity of these liposomes, their unique morphology and their unprecedented *in vivo* behavior provide new opportunities and design guidelines to develop nanomedicines capable of exploiting endogenous plasma lipid transport and metabolism pathways.

While the demonstrated targeting of any (or all) triglyceride lipase family member(s) represents a significant advance in the development of targeted nanoparticles, our results point to a specific targeting preference for EL over LPL and HL. In mice, EL expression is dynamically restricted in both time and space. This is most evident during embryonic stages when high EL expression is observed, particularly in the brain, between embryonic days E8.5 and E11.5 but not at later developmental stages.[67] In healthy adult mice, EL expression is mainly restricted to the lungs, liver, spleen, testes and ovaries (during pregnancy) and is particularly high in the placenta of pregnant mice.[15, 16, 67, 68] A similar restricted pattern of EL expression has been reported in humans.[15] In the diseased state, and beyond its determinant role in regulating plasma HDL-cholesterol levels,[69, 70] EL plays an important role in the initiation and proliferation of various cancers, including breast, gastric and testicular cancers.[71-73] In these cases, aberrant EL overexpression within the tumor environment may be triggered by severe oxidative stress, which in turn leads to endothelial cell migration and angiogenesis through activation of sphigosine-1-phosphate (S1P).[74] Overall, EL plays a crucial angiogenic role in both the healthy and diseased states and, given its restricted expression, notably within the reproductive organs and tumor microenvironment, could be a highly lucrative target for new nanoparticle-based cell-specific therapies.

In conclusion, cell specific targeting is a central tenet to the realization of the widespread use of nanomedicines in the clinic. However, it remains a largely unmet goal. To realize this goal, it is becoming increasingly clear that a thorough understanding of the fundamental nano-bio interactions involved is an absolute requirement. To this end, this work once again highlights the unique opportunities the zebrafish embryo can offer within nanomedicine discovery and development pipelines. Beyond the already reviewed benefits of size, transparency, fecundity and ease of genetic manipulation,[75] in this case, the very discovery of ('irrational') PAP3 liposomes was only possible due to our ability to visualize large numbers of liposome formulations *in vivo* at high resolution and across an entire living organism. Arising from an unexpected molecular rearrangement of a proposed cationic lipid (**Supplementary Figure 12**), the discovery of PAP3 liposomes was ultimately pure serendipity.

5.5 Materials and Methods

General reagents

1,2-dioleoyl-*sn*-glycero-3-phosphocholine(DOPC),1,2-distearoyl-*sn*-glycero-3phosphocholine (DSPC), 1,2-dioleoyl-*sn*-glycero-3-phosphoethanolamine-N-(lissamine rhodamine B sulfonyl) (DOPE-LR) and NOTA-Bz-SCN-C18 (custom made), were purchased from Avanti Polar Lipids (Alabaster, AL, US). Additional DSPC was purchased from Lipoid GmbH. pHrodo™ Red, succinimidyl ester (pHrodo™ Red, SE) was purchased from Thermo Fisher Scientific. DOPE-pHrodo was synthesized as previously reported.[76] All other chemical reagents were purchased at the highest grade available from Sigma Aldrich and used without further purification. All solvents were purchased from Biosolve Ltd. Ultrapure MilliQ® water, purified by a MilliQ Advantage A10 water purification system from MilliPore, was used throughout. DOaG & DOG lipid lipids were synthesized and characterised in house.

Liposome formulation

Liposomes were formulated by extrusion or by ethanol injection method in ddH_2O at a total lipid concentration of 5mM, unless otherwise stated. In the case of extrusion, individual lipids as stock solutions (1-10 mM) in chloroform, were combined to the desired molar ratios and dried to a thin film, first under N_2 stream, then >1 h under vacuum. Lipid films were hydrated in 1mL ddH2O above the T_m of all lipids (65-70 ^oC), with gentle vortexing if necessary, to form a

suspension. Large unilamellar vesicles were formed through extrusion (mini extruder, Avanti Polar Lipids) above the T_m of all lipids (*i.e.* 65-70 °C). Hydrated lipids were passed 11 times through 2 x 400 nm polycarbonate (PC) membranes (Nucleopore Track-Etch membranes, Whatman), followed by 11 times through 2 x 100 nm PC membranes. All liposomes were stored at 4 °C and used within 1 week. In the case of ethanol injection, lipid films were re-dissolved in ethanol to a total lipid concentration of 50 mM. Using a glass micro-syringe (Hamilton, syringe series 700, volume 50 or 500ul) the ethanolic solution was rapidly injected in a glass vial containing 0.5mL or 1mL ddH_2O (1:10 v:v; EtOH:H_2O) at 70°C, under constant vigorous stirring (650rpm), to form large unilamellar vesicles. Liposomes were then transferred to a dialysis tube (Spectrum labs, 3.5k MWCO) or a dialysis cassette (slide-A-Lyzer™ 3.5k MWCO, Thermo Fisher Scientific) and dialyzed against ddH_2O overnight at 4°C, to ensure complete ethanol removal. All liposomes were stored at 4°C and used within 1 week.

Size and zeta potential measurements

Particle size and zeta potentials were measured using a Malvern Zetasizer Nano ZS. For DLS (operating wavelength = 633 nm), measurements were carried out at room temperature in water at a total lipid concentration of approx. 100 µM. Zeta potentials were measured at 500 µM total lipid concentration, using a dip-cell electrode (Malvern), at room temperature. For liposomes formulated in water, aq. NaCl was added to the liposome solution to a final concentration of 10 mM NaCl before zeta potential measurement. All reported DLS measurements and zeta potentials are the average of three measurements.

CryoTEM and 3D tomography

Liposomes (3 µL, 5 mM total lipid concentration) were applied to a freshly glow-discharged carbon 200 mesh Cu grid (Lacey carbon film, Electron Microscopy Sciences, Aurion, Wageningen, The Netherlands). Grids were blotted for 3 s at 99% humidity in a Vitrobot plunge-freezer (FEI VitrobotTM Mark III, Thermo Fisher Scientific). Cryo-EM images were collected on a Talos L120C or a KRIOS (NeCEN, Leiden University) operating at 120 kV or 300kV, respectively. In the case of Talos, images were recorded manually at a nominal magnification of 17500x or 28000x yielding a pixel size at the specimen of 5.83 or 3.56 ångström (Å), respectively. In the case of KRIOS, images were recorded manually at a nominal magnification of 33000x yielding a pixel size at the specimen of 3.48 Å. Alternatively, imaging and cryo-ET was performed on a Titan Krios operating at 300kV (TU Eindhoven). Images were recorded manually at a nominal

magnification of 6500x or 24000x yielding a pixel size at the specimen of 13.87 or 3.86 Å, respectively. Tomographic tilt series acquisition was performed with Inspect3D software (Thermo Fisher Scientific) with a total electron dose of less than 100 e/nm^2. Alignment and reconstruction of the series were performed using IMOD[77] and 3D analysis software Avizo 9 (Thermo Fisher Scientific).

Zebrafish husbandry and injections

Zebrafish (*Danio rerio*, strain AB/TL) were maintained and handled according to the guidelines from the Zebrafish Model Organism Database (http://zfin.org) and in compliance with the directives of the local animal welfare committee of Leiden University. Fertilization was performed by natural spawning at the beginning of the light period, and eggs were raised at 28.5 °C in egg water (60 ug/ mL Instant Ocean sea salts). The following previously established zebrafish lines were used: Tg*(cldn5b:*eGFP*),*[33] Tg*(kdrl:*eGFP*)*^{s843},[78] Tg*(mpeg1:*GFP*)*^{gl22},[79] Tg*(mpeg1:*mCherry*)*^{gl23}.[79] Liposomes were injected into 54-120 hours post fertilization zebrafish embryos using a modified microangiography protocol.[5] Embryos were anesthetized in 0.01% tricaine and embedded in 0.4% agarose containing tricaine before injection. To improve reproducibility of microangiography experiments, 1 nl volume were calibrated and injected into the sinus venosus/Duct of Cuvier or the primary head sinus. A small injection space was created by penetrating the skin with the injection needle and gently pulling the needle back, thereby creating a small pyramidal space in which the liposomes and polymers were injected. Successfully injected embryos were identified through the backward translocation of venous erythrocytes and the absence of damage to the yolk ball.

Confocal imaging acquisition and editing

Zebrafish embryos were randomly picked from a dish of 20-60 successfully injected embryos. Confocal z-stacks were captured on a Leica TCS SPE or SP8 confocal microscope, using a 10x air objective (HCX PL FLUOTAR), a 40x water-immersion objective (HCX APO L) or 63x water-immersion objective (HC PL APO CS). For whole-embryo views, 3 overlapping z-stacks were captured to cover the complete embryo. Laser intensity, gain and offset settings were identical between stacks and experiments. Images were processed and quantified using the Fiji distribution of ImageJ.[80, 81] Confocal image stacks (raw data) are available upon request.

Protein corona analysis

Protein corona was analyzed as described in reference.[57] Briefly, PAP3 liposomes were formulated incorporating 5 mol% of the IKS02 photoaffinity lipid probe and incubated in human serum. Protein adsorbed to the surface of the liposomes were identified *in situ* by cross linking proteins to the diazirine group of the IK probe with light irradiation. Afterwards, the captured proteins were isolated and quantified with LC-MS/MS.

Studies in mice

General

Female mice weighting *ca.* 18-20 g (BALB/cJRj, 6-8 weeks, Janvier; see below for number of animals) were used. The animals were maintained and handled in accordance with the Guidelines for Accommodation and Care of Animals (European Convention for the Protection of Vertebrate Animals Used for Experimental and Other Scientific Purposes) and internal guidelines. All experimental procedures were approved by the Ethical Committee of CIC biomaGUNE and by local authorities (Diputación Foral de Guipúzcoa) before conducting experimental work.

Radiolabeling of liposomes

PAP3 liposomes with 12.5 mM total lipid concentration were made by ethanol injection as described above with only difference that 0.2 mol% of NOTA-Bz-SCN-C18 (custom made, Avanti Polar Lipids) was added to the lipid film. Additionally, the required total volume of liposomes was made in two batches of 500 µl to ensure avoidance of aggregation. After formation of particles and removal of ethanol, $^{64}CuCl_2$ in 0.1 M aq. ammonium acetate pH=5.5 was added to the liposome solution and the mixture was incubated at room temperature (20 mins) (1:4 v/v ammonium acetate/liposomes). Subsequently, the free $^{64}CuCl_2$ was removed by size exclusion chromatography (NAP™-25 columns Sephadex™, GE Healthcare) equilibrated with 10 mM Tris buffer pH=7.4. Elution fractions of 500 µl containing the radiolabeled liposomes were collected from the SEC column and their radioactivity was checked using a dose calibrator (CPCRC-25R, Capintec Inc., NJ, USA). The fraction containing the higher concentration of radioactivity was used for subsequent *in vivo* imaging and *ex vivo* studies.

PET imaging studies

For PET imaging studies, anesthesia was induced by inhalation of 3% isoflurane in pure O_2 and maintained by 1.5-2% isofluorane in 100% O_2. With the animal under anesthesia, the labelled liposomes were injected *via* one of the lateral tail veins (930±50 kBq/100 µL; n=3). Dynamic whole-body images (20 min duration) were acquired list-mode in one bed position in a 511 keV ± 30% energetic window immediately after administration of the labelled liposomes using a MOLECUBES β-CUBE scanner. Static 10 min images were also acquired at 2h, 6h and 24f after administration. After each PET scan, whole body high resolution computed tomography (CT) acquisitions were performed on the MOLECUBES X-CUBE scanner, to provide anatomical information as well as the attenuation map for the later reconstruction of the PET images. Dynamic PET images were reconstructed with OSEM-3D iterative algorithm, using the following frames: 4 × 30 s, 4 × 60 s, 4 × 120 s, 2 × 180 s. Static images were reconstructed as a single frame using the same method. Images were analyzed using π-MOD image analysis software (π-MOD Technologies Ltd, Zurich, Switzerland). With that aim, volumes of interest (VOIs) were manually drawn in major organs, namely brain, lungs, kidneys, spleen, stomach, liver, bladder and heart, using the CT images for anatomical reference, and decay–corrected time–activity curves were obtained. Values were normalized to VOI volume and injected activity and values were expressed as percentage of injected dose per cubic centimeter of tissue (%ID/cm^3).

Ex vivo biodistribution studies

Animals (n=3 per compound and time point) were anesthetized with isoflurane 3% isoflurane in pure O_2 and maintained by 1.5-2% isoflurane in 100% O_2. A solution containing the labelled liposomes (730 ± 140 kBq/100 µl) was injected through one of the lateral tail veins. Animals were recovered from anesthesia and at pre-determined time points (t=10 min, and 2, 6 and 24 h), animals were anesthetized again and sacrificed by perfusion using saline solution and brain, liver, kidneys, spleen, lungs, heart, and stomach were quickly removed and rinsed with water. The amount of radioactivity in each organ was measured in an automatic gamma counter (2470 Wizard, PerkinElmer). Blood samples were obtained just before perfusion. Part of the blood was processed to separate the plasma, which was also counted in the gamma counter. Results were normalized to injected dose and organ weight to express the results as percentage of injected dose per gram of tissue (%ID/g).

5.6 Abbreviations

Å	Ångström
ApoA	apolipoprotein A
BA	basilar artery
BBB	blood brain barrier
bECs	brain endothelial cells
CE	cholesteryl esters
CHT	caudal hematopoietic tissue
CryoTEM	Cryo-transmission electron microscopy
CV	caudal vein
DLV	dorsal longitudinal vein
DOPE-LR	1,2-dioleoyl-*sn*-glycero-3-phosphoethanolamine-N-(lissamine rhodamine B sulfonyl)
DSPC	1,2-distearyl-*sn*-glycero-3-phosphocholine
DOaG	2-hydroxy-3-oleamidopropyl oleate
dpf	days post fertilization
EL	endothelial lipase
FAs	fatty acids
HDL	high density lipoproteins
HL	hepatic lipase
HSPG	heparan sulfate proteoglycan
hpi	hour(s) post injection
i.v.	Intravenously
LCAT	lecithin cholesterol acyltransferase
LDL(R)	low density lipoproteins (receptor)
LNP	lipid nanoparticle
LPL	lipoprotein lipase
LSECs	liver sinusoidal endothelial cells
Ms(A/V)	mesencephalic artery/vein
MCeV	middle cerebral vein
MMCtA	middle mesencephalic central artery
PMBC	primordial midbrain channel
PHBC	primordial hindbrain channel
SECs	scavenging endothelial cells
TG	triglycerides
VLDL	very low density lipoproteins
wt	wildtype

5.7 Supporting Information

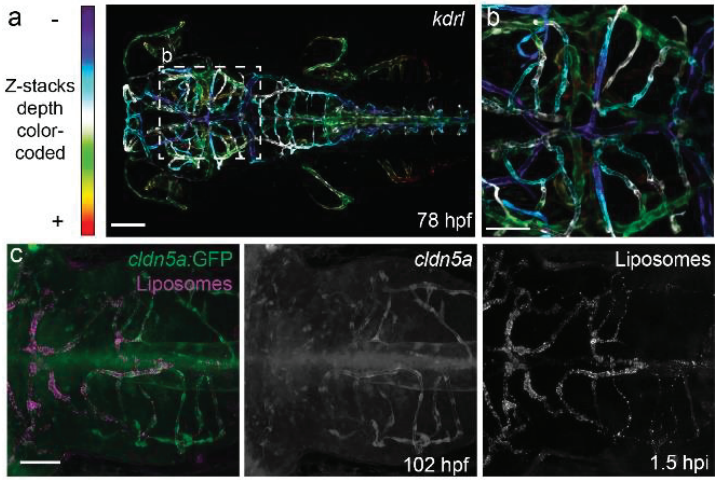

Supplementary Figure 1. Zebrafish embryo ECs in dorsal view and biodistribution of PAP3 liposomes in Tg*(cldn5a:*eGFP). (a-b) Z-stacks depth color-coded of a Tg(*kdrl*:GFP), dorsal view, at 78 hours post injection (hpi). Thermal colored scale, blue (dorsal) up to red (ventral). **(c)** Biodistribution of PAP3 liposomes (5 mM containing 0.2 mol% DOPE-LR, in magenta or gray) after 1.5 hpi in dorsal view. bECs, zoom in (magnification 40x) the hindbrain region showing correlation of PAP3 liposomes (magenta/gray) with expression of *cldn5a* at ~102 hpf. (Whole embryo, 10x in **Figure 2j**). Scale bars: 100 µm (a) and 50 µm (b-c).

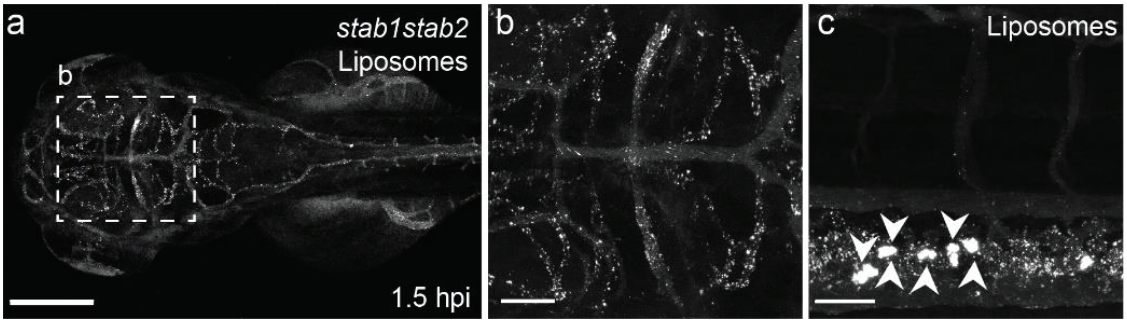

Supplementary Figure 2. Biodistribution of PAP3 liposomes in *stab1stab2* double knockout zebrafish embryo. (a) PAP3 liposomes (5 mM containing 0.2 mol% DOPE-LR, in gray) biodistribution in dorsal view (magnification 10x) *i.v.* injected in zebrafish line stab1^{ibl3}stab2^{ibl1},[30] 1.5 hpi at ~76 hpf. **(b)** Zoom in (magnification 40x) of bECs **(c)** Caudal region in lateral view (magnification 40x) showing accumulation of PAP3 liposomes in scavenging endothelial cells (SECs), expressing Stabilin-1 and Stabilin-2, analogous to liver sinusoidal endothelial cells in mice[29] and in apparent blood-exposed macrophages (white arrows). Scale bar: 200 µm (a) and 50 µm (b-c).

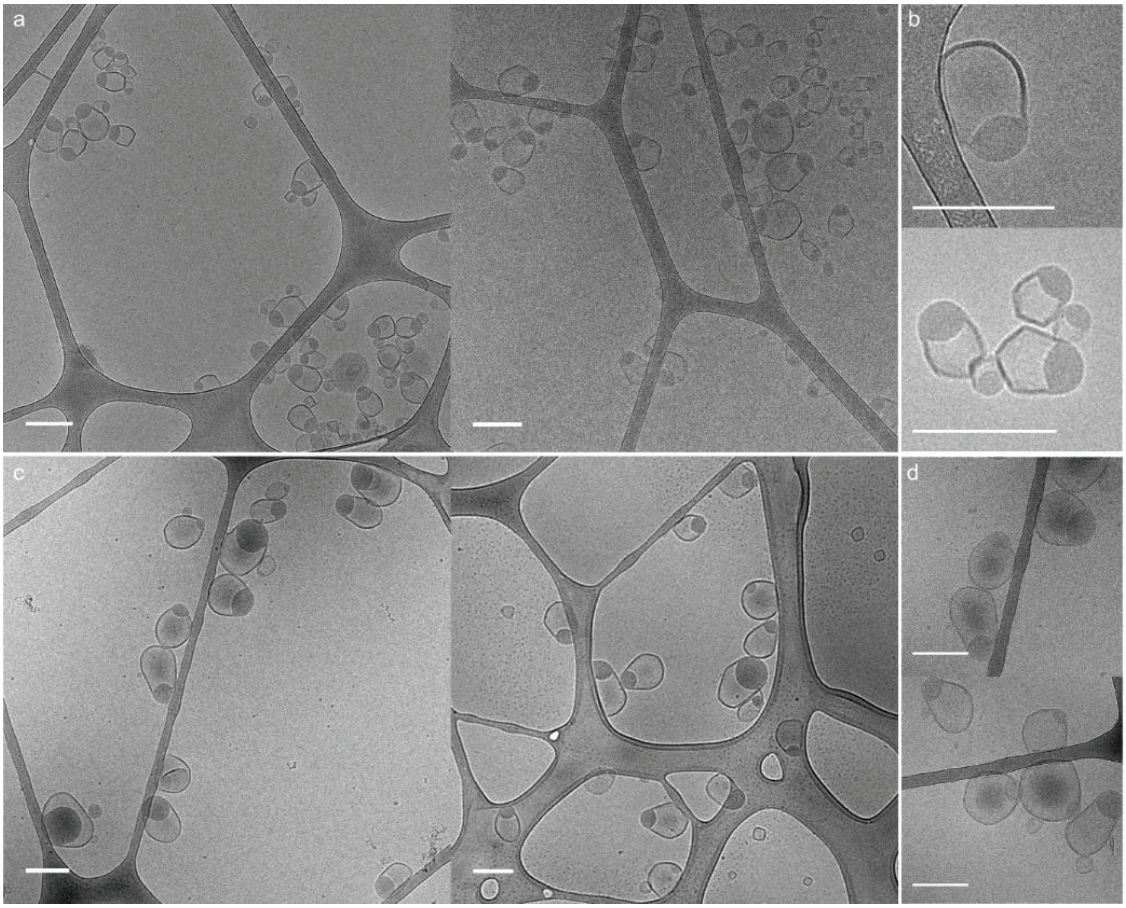

Figure Supplementary 3. CryoTEM images of 'parachute' PAP3 liposomes formulated by two methods. (a-b) PAP3 liposomes formulated by ethanol injection method. **(c-d)** PAP3 liposomes formulated by extrusion method. Scales bars: 200 nm.

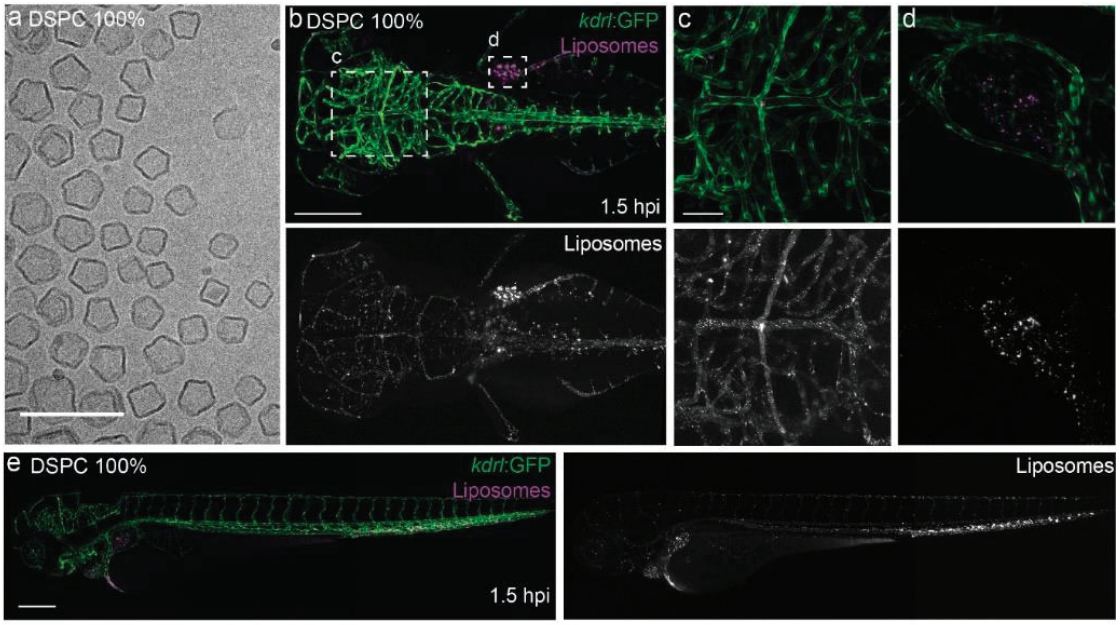

Supplementary Figure 4. CryoTEM and biodistribution of DSPC liposomes in zebrafish embryo. (a) CryoTEM images of DSPC liposomes. **(b)** Biodistribution of DSPC liposomes (5 mM containing 0.2 mol% DOPE-LR, in magenta or gray) in Tg(*kdrl:*GFP) transgenic line, at 3 dpf, 1.5 hpi in dorsal view (magnification 10x). **(c)** Brain endothelial cells (bECs) at tissue level (magnification 40x) in dorsal view. **(d)** Liver endothelium (magnification 40x), in lateral view. **(e)** Whole body lateral view (same fish, magnification 10x). Liposomes prepared by extrusion. Scale bars: 200 nm (cryoTEM), 200 μm (dorsal and lateral views) and 50 μm (tissue level).

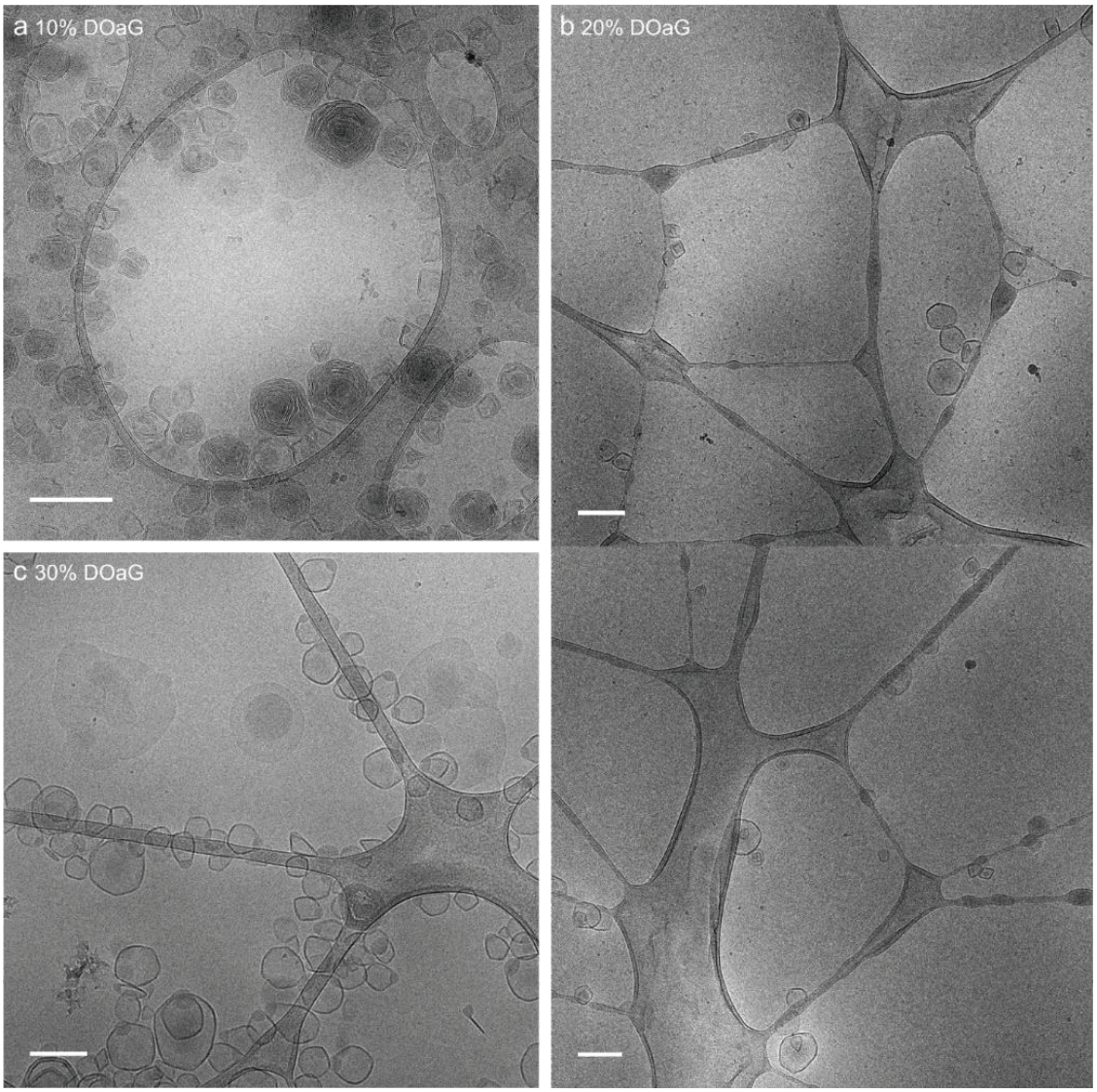

Supplementary Figure 5. CryoTEM images of PAP3 liposomes formulated at varying molar ratios. (a) Liposomes composed of DSPC and 10 mol%, **(b)** 20 mol% (2 images included because of low population of particles in an individual image), and **(c)** 30 mol% DOaG. Scales bars: 200 nm.

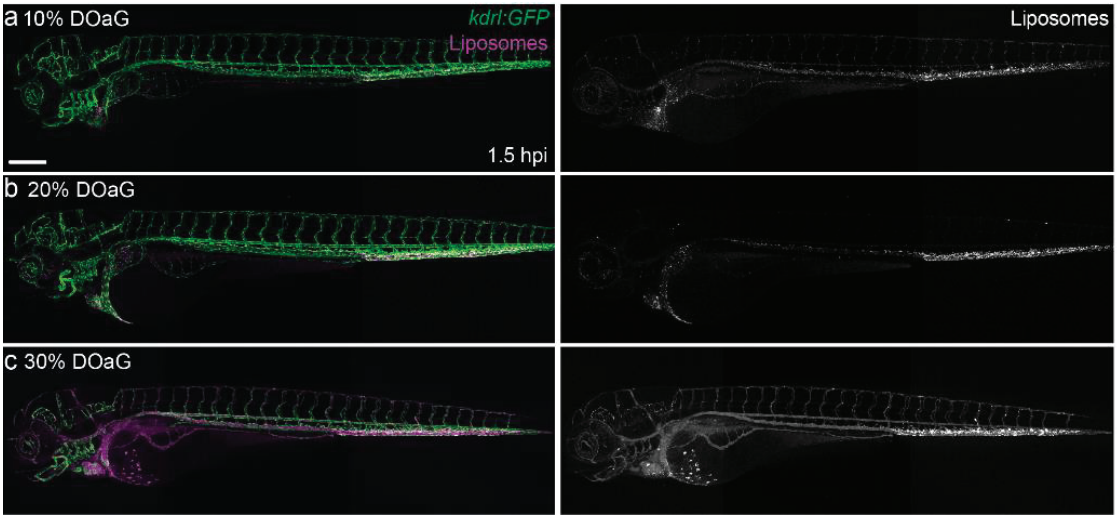

Supplementary Figure 6. Biodistribution of PAP3 liposomes formulated at varying molar ratios. a) Liposomes (5 mM containing 0.2 mol% DOPE-LR, magenta or gray) composed of DSPC and 10 mol%, **b)** 20 mol%, or **c)** 30 mol% DOaG in a Tg(*kdrl:*GFP) embryo at 78 hpf, 1.5 hpi (10x magnification). Scale bar 200 μm.

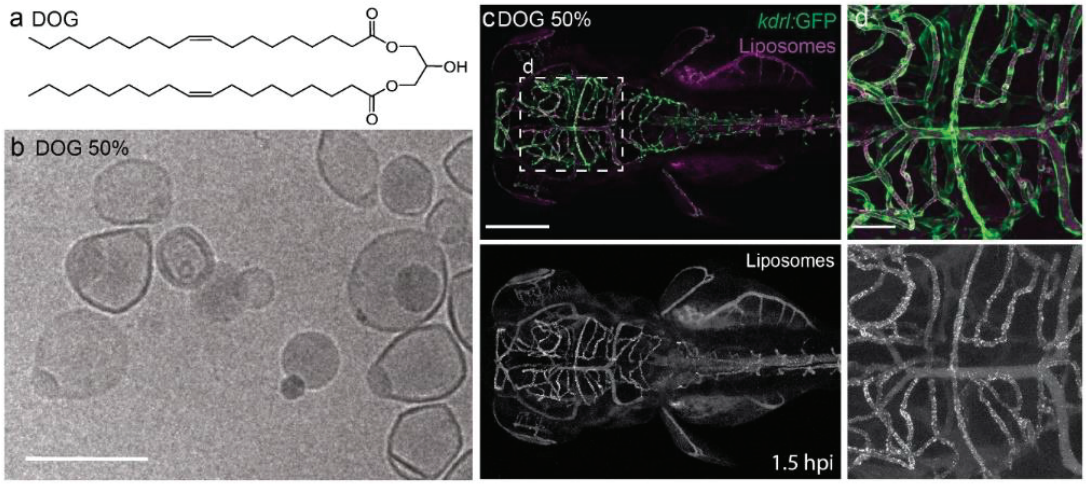

Supplementary Figure 7. CryoTEM and biodistribution of DSPC and DOG containing liposomes. (a) Chemical structure of 1,3-DiOleoyl Glycerol (DG(18:1/0:0/18:1) **(b)** CryoTEM of liposomes containing DSPC and DOG in equal ratios. **(c)** Biodistribution of DSPC-DOG (5 mM containing 0.2 mol% DOPE-LR, in magenta or gray) in zebrafish at 78 hpf, 1.5 hpi in dorsal view. **(d)** bECs (40x magnification). Scale bars: 200 nm (cryoTEM), 200 μm (dorsal view) and 50 μm (tissue level).

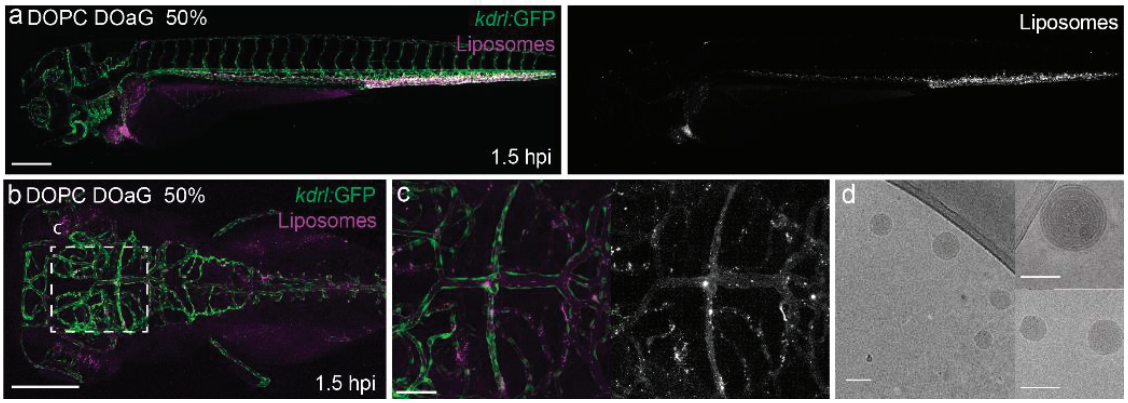

Supplementary Figure 8. DOPC-DOaG liposomes in zebrafish embryo. (a) Biodistribution of liposomes composed of DOPC and DOaG in equal ratios (magenta or gray) in Tg(*kdrl*:GFP) transgenic line, at 78 hpf, 1.5 hpi in lateral view. **(b)** Dorsal view (10x magnification.) **(c)** bECs, at tissue level (40x magnification). **(d)** CryoTEM images of DOPC:DOaG liposomes showing multilamellar or solid lipid-like morphology. Liposomes formulated by ethanol injection, concentration 5 mM containing 0.2 mol% DOPE-LR. Extrusion was not possible with this formulation. Scale bars: 200 µm (dorsal and lateral views), 50 µm (tissue level) and 100 nm for CryoTEM.

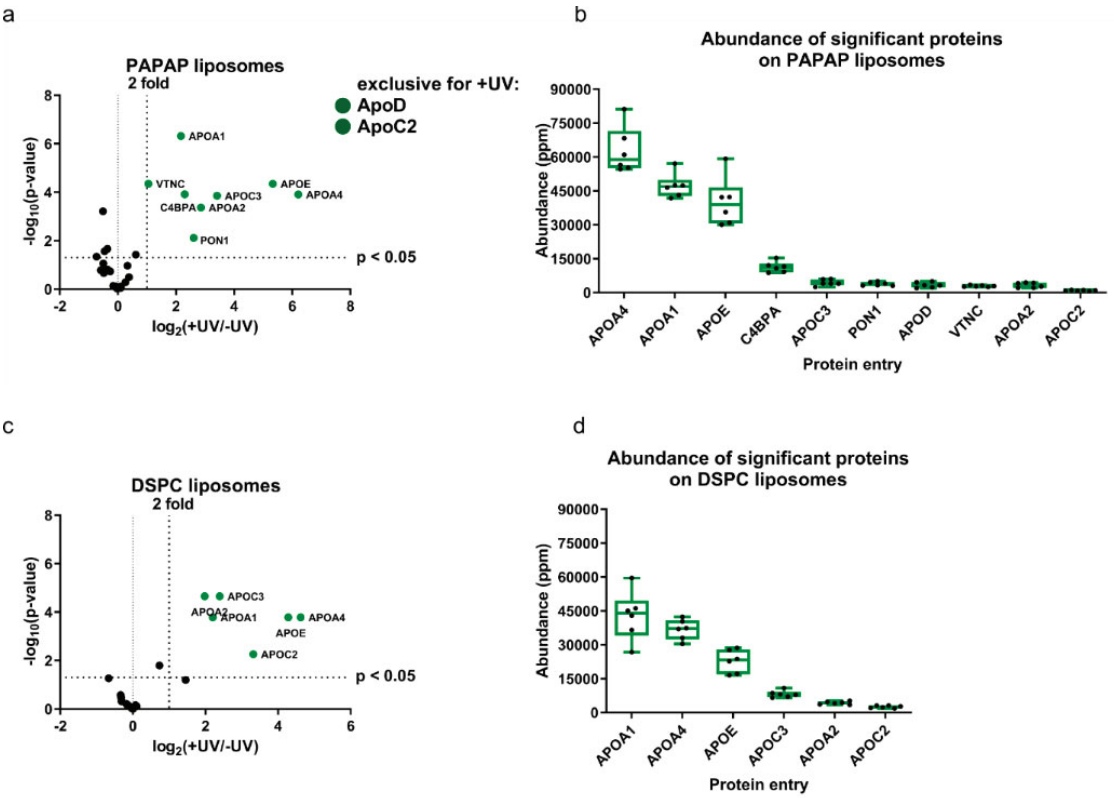

Supplementary Figure 9. Identification of the PAP3 liposome protein corona, isolated via photoaffinity method. (a, c) Volcano plots of enrichment over background (log_2(+UV/-UV) plotted against the statistical significance of this comparison (-log_{10}(*p*-

value)) of PAP3 and DSPC liposomes respectively. Proteins meeting all selection criteria labeled in green. Proteins without background labeling are listed as exclusive for +UV. **(b, d)** Abundance plots of proteins (replicate abundancies of the top10 proteins (ppm) withing the +UV samples) identified in PAP3 and DSPC liposomes respectively. Liposomes with affinity probe (IKS02 5mol%) incorporated into the liposome membrane made by extrusion.

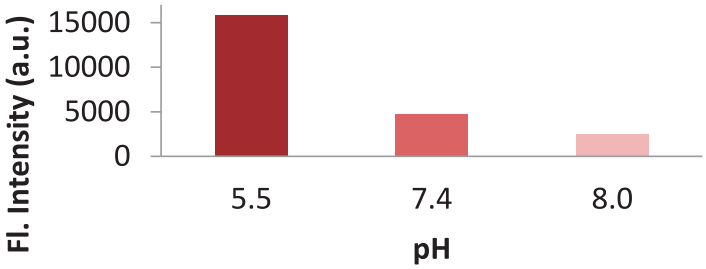

Supplementary Figure 10. Fluorescence intensity of PAP3 liposomes containing 0.5 %mol DOPE-pHrodo™ at different pH (5.5, 7.4 and 8).

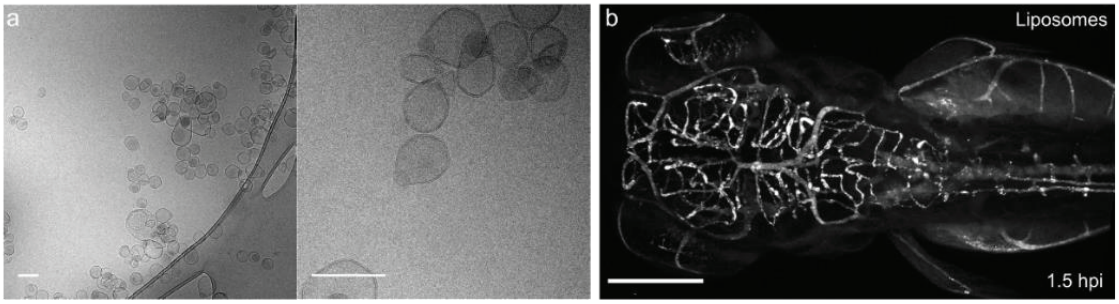

Supplementary Figure 11. CryoTEM and biodistribution of ^{64}Cu - PAP3 liposomes containing NOTA-Bz-SCN-C18. (a) CryoTEM images of PAP3 liposomes containing 0.2%mol NOTA-Bz-SCN-C18 after Cu chelation (stable Cu isotope). **(b)** Biodistribution of PAP3 liposomes containing 0.2%mol NOTA-Bz-SCN-C18 after ^{64}Cu chelation in zebrafish. Sample administered in mice was later injected in zebrafish to ensure bEC targeting was retained. Sample was injected in zebrafish two weeks later to ensure radioactivity decay. Scale bars : 200 nm (cryoTEM), 200 µm (dorsal view).

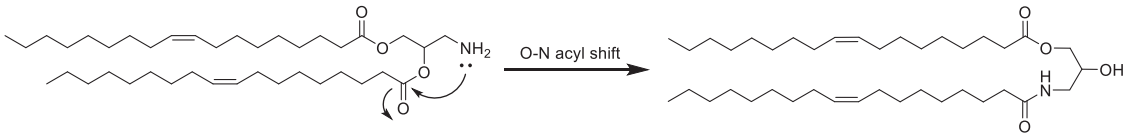

Supplementary Figure 12. O-N intramolecular acyl migration. Cationic lipid originally used for another project underwent rearrangement resulting in DOaG lipid.

Supplementary Table 1. Physicochemical properties of liposomes

Liposomes	Preparation method	Size (nm)	PDI	Stability*
DSPC	Extrusion	± 110.9	0.062	> month
PAP3 liposomes (10%DOaG)	Ethanol injection	± 137.5	0.179	n/a
PAP3 liposomes (20%DOaG)	Ethanol injection	± 107.5	0.181	n/a
PAP3 liposomes (30%DOaG)	Ethanol injection	± 136.5	0.281	n/a
PAP3 liposomes (50%DOaG)	Ethanol injection	± 123.0	0.218	~7 days
	Extrusion	± 153.1	0.114	~7 days
DSPC:DOaG:IKS02 (45:50:5)	Extrusion	± 129.4	0.163	n/a
DSPC:DOG (50:50)	Extrusion	± 161.7	0.318	~7days
DOPC:DOaG (50:50)	Ethanol Injection	± 200.2	0.141	~2 days
DSPC:DOaG:NOTA (49.9:49.9:0.2)	Ethanol Injection	± 174.0	0.159	~5 days
DSPC:DOaG:NOTA (49.9:49.9:0.2) *labelled with Cu^{2+} (cold)*	Ethanol Injection	± 260.8	0.231	~1day
DSPC:DOaG:DOPE-pHrodo:NBD (49.5 :49.5 :0.5 :0.5)	Extrusion	± 126.2	0.227	n/a

*Determined by dynamic light scattering (DLS) measurements for each formulation, over the period of 2,3,7,14 and 30 days.

5.8 References

1. Feingold, K. R., Introduction to Lipids and Lipoproteins. In *Endotext*, Feingold, K. R.; Anawalt, B.; Boyce, A.; Chrousos, G.; de Herder, W. W.; Dhatariya, K.; Dungan, K.; Grossman, A.; Hershman, J. M.; Hofland, J.; Kalra, S.; Kaltsas, G.; Koch, C.; Kopp, P.; Korbonits, M.; Kovacs, C. S.; Kuohung, W.; Laferrere, B.; McGee, E. A.; McLachlan, R.; Morley, J. E.; New, M.; Purnell, J.; Sahay, R.; Singer, F.; Stratakis, C. A.; Trence, D. L.; Wilson, D. P., Eds. South Dartmouth (MA), 2000.
2. Akinc, A.; Maier, M. A.; Manoharan, M.; Fitzgerald, K.; Jayaraman, M.; Barros, S.; Ansell, S.; Du, X.; Hope, M. J.; Madden, T. D.; Mui, B. L.; Semple, S. C.; Tam, Y. K.; Ciufolini, M.; Witzigmann, D.; Kulkarni, J. A.; van der Meel, R.; Cullis, P. R., The Onpattro story and the clinical translation of nanomedicines containing nucleic acid-based drugs. *Nat Nanotechnol* **2019,** *14* (12), 1084-1087.
3. Akinc, A.; Querbes, W.; De, S.; Qin, J.; Frank-Kamenetsky, M.; Jayaprakash, K. N.; Jayaraman, M.; Rajeev, K. G.; Cantley, W. L.; Dorkin, J. R., et al., Targeted delivery of RNAi therapeutics with endogenous and exogenous ligand-based mechanisms. *Mol Ther* **2010,** *18* (7), 1357-1364.
4. Ference, B. A.; Ginsberg, H. N.; Graham, I.; Ray, K. K.; Packard, C. J.; Bruckert, E.; Hegele, R. A.; Krauss, R. M.; Raal, F. J.; Schunkert, H., et al., Low-density lipoproteins cause atherosclerotic cardiovascular disease. 1. Evidence from genetic, epidemiologic, and clinical studies. A consensus statement from the European Atherosclerosis Society Consensus Panel. *Eur Heart J* **2017,** *38* (32), 2459-2472.
5. Goldstein, J. L.; Brown, M. S., A century of cholesterol and coronaries: from plaques to genes to statins. *Cell* **2015,** *161* (1), 161-172.
6. Fielding, C. J.; Fielding, P. E., Molecular physiology of reverse cholesterol transport. *J Lipid Res* **1995,** *36* (2), 211-228.
7. Allan, C. M.; Fidge, N. H.; Morrison, J. R.; Kanellos, J., Monoclonal antibodies to human apolipoprotein AI: probing the putative receptor binding domain of apolipoprotein AI. *Biochem J* **1993,** *290 (Pt 2)*, 449-455.
8. Vadiveloo, P. K.; Allan, C. M.; Murray, B. J.; Fidge, N. H., Interaction of apolipoprotein AII with the putative high-density lipoprotein receptor. *Biochemistry* **1993,** *32* (36), 9480-9485.
9. Hussain, M. M.; Strickland, D. K.; Bakillah, A., The mammalian low-density lipoprotein receptor family. *Annu Rev Nutr* **1999,** *19*, 141-172.
10. Subbaiah, P. V.; Albers, J. J.; Chen, C. H.; Bagdade, J. D., Low density lipoprotein-activated lysolecithin acylation by human plasma lecithin-cholesterol acyltransferase. Identity of lysolecithin acyltransferase and lecithin-cholesterol acyltransferase. *J Biol Chem* **1980,** *255* (19), 9275-9280.
11. Shen, Y.; Lookene, A.; Zhang, L.; Olivecrona, G., Site-directed mutagenesis of apolipoprotein CII to probe the role of its secondary structure for activation of lipoprotein lipase. *J Biol Chem* **2010,** *285* (10), 7484-7492.
12. Amar, M. J.; Sakurai, T.; Sakurai-Ikuta, A.; Sviridov, D.; Freeman, L.; Ahsan, L.; Remaley, A. T., A novel apolipoprotein C-II mimetic peptide that activates lipoprotein lipase and decreases serum triglycerides in apolipoprotein E-knockout mice. *J Pharmacol Exp Ther* **2015,** *352* (2), 227-235.
13. Mead, J. R.; Irvine, S. A.; Ramji, D. P., Lipoprotein lipase: structure, function, regulation, and role in disease. *J Mol Med (Berl)* **2002,** *80* (12), 753-769.
14. Connelly, P. W., The role of hepatic lipase in lipoprotein metabolism. *Clin Chim Acta* **1999,** *286* (1-2), 243-255.
15. Jaye, M.; Lynch, K. J.; Krawiec, J.; Marchadier, D.; Maugeais, C.; Doan, K.; South, V.; Amin, D.; Perrone, M.; Rader, D. J., A novel endothelial-derived lipase that modulates HDL metabolism. *Nat Genet* **1999,** *21* (4), 424-428.
16. Hirata, K.; Dichek, H. L.; Cioffi, J. A.; Choi, S. Y.; Leeper, N. J.; Quintana, L.; Kronmal, G. S.; Cooper, A. D.; Quertermous, T., Cloning of a unique lipase from endothelial cells extends the lipase gene family. *J Biol Chem* **1999,** *274* (20), 14170-14175.
17. Fuki, I. V.; Blanchard, N.; Jin, W.; Marchadier, D. H.; Millar, J. S.; Glick, J. M.; Rader, D. J., Endogenously produced endothelial lipase enhances binding and cellular processing of plasma lipoproteins via heparan sulfate proteoglycan-mediated pathway. *J Biol Chem* **2003,** *278* (36), 34331-34338.
18. Santamarina-Fojo, S.; Dugi, K. A., Structure, function and role of lipoprotein lipase in lipoprotein metabolism. *Curr Opin Lipidol* **1994,** *5* (2), 117-125.
19. Landin, B.; Nilsson, A.; Twu, J. S.; Schotz, M. C., A role for hepatic lipase in chylomicron and high density lipoprotein phospholipid metabolism. *J Lipid Res* **1984,** *25* (6), 559-563.

20. Dugi, K. A.; Dichek, H. L.; Santamarina-Fojo, S., Human hepatic and lipoprotein lipase: the loop covering the catalytic site mediates lipase substrate specificity. *J Biol Chem* **1995,** *270* (43), 25396-25401.
21. McCoy, M. G.; Sun, G. S.; Marchadier, D.; Maugeais, C.; Glick, J. M.; Rader, D. J., Characterization of the lipolytic activity of endothelial lipase. *J Lipid Res* **2002,** *43* (6), 921-929.
22. Yu, J. E.; Han, S. Y.; Wolfson, B.; Zhou, Q., The role of endothelial lipase in lipid metabolism, inflammation, and cancer. *Histol Histopathol* **2018,** *33* (1), 1-10.
23. Ishida, T.; Choi, S.; Kundu, R. K.; Hirata, K.; Rubin, E. M.; Cooper, A. D.; Quertermous, T., Endothelial lipase is a major determinant of HDL level. *J Clin Invest* **2003,** *111* (3), 347-355.
24. Paradis, M. E.; Lamarche, B., Endothelial lipase: its role in cardiovascular disease. *Can J Cardiol* **2006,** *22 Suppl B*, 31B-34B.
25. Jin, W.; Millar, J. S.; Broedl, U.; Glick, J. M.; Rader, D. J., Inhibition of endothelial lipase causes increased HDL cholesterol levels in vivo. *J Clin Invest* **2003,** *111* (3), 357-362.
26. Strauss, J. G.; Zimmermann, R.; Hrzenjak, A.; Zhou, Y.; Kratky, D.; Levak-Frank, S.; Kostner, G. M.; Zechner, R.; Frank, S., Endothelial cell-derived lipase mediates uptake and binding of high-density lipoprotein (HDL) particles and the selective uptake of HDL-associated cholesterol esters independent of its enzymic activity. *Biochem J* **2002,** *368* (Pt 1), 69-79.
27. Sieber, S.; Grossen, P.; Detampel, P.; Siegfried, S.; Witzigmann, D.; Huwyler, J., Zebrafish as an early stage screening tool to study the systemic circulation of nanoparticulate drug delivery systems in vivo. *J Control Release* **2017,** *264*, 180-191.
28. Arias-Alpizar, G.; Kong, L.; Vlieg, R. C.; Rabe, A.; Papadopoulou, P.; Meijer, M. S.; Bonnet, S.; Vogel, S.; van Noort, J.; Kros, A.; Campbell, F., Light-triggered switching of liposome surface charge directs delivery of membrane impermeable payloads in vivo. *Nat Commun* **2020,** *11* (1), 3638.
29. Campbell, F.; Bos, F. L.; Sieber, S.; Arias-Alpizar, G.; Koch, B. E.; Huwyler, J.; Kros, A.; Bussmann, J., Directing Nanoparticle Biodistribution through Evasion and Exploitation of Stab2-Dependent Nanoparticle Uptake. *ACS Nano* **2018,** *12* (3), 2138-2150.
30. Arias-Alpizar, G.; Koch, B.; Hamelmann, N. M.; Neustrup, M. A.; Paulusse, J. M. J.; Jiskoot, W.; Kros, A.; Bussmann, J., Stabilin-1 is required for the endothelial clearance of small anionic nanoparticles. *Nanomedicine: Nanotechnology, Biology and Medicine* **2021**, 102395.
31. Hayashi, Y.; Takamiya, M.; Jensen, P. B.; Ojea-Jiménez, I.; Claude, H.; Antony, C.; Kjaer-Sorensen, K.; Grabher, C.; Boesen, T.; Gilliland, D.; Oxvig, C.; Strähle, U.; Weiss, C., Differential Nanoparticle Sequestration by Macrophages and Scavenger Endothelial Cells Visualized in Vivo in Real-Time and at Ultrastructural Resolution. *ACS Nano* **2020,** *14* (2), 1665-1681.
32. Quinonez-Silvero, C.; Hubner, K.; Herzog, W., Development of the brain vasculature and the blood-brain barrier in zebrafish. *Dev Biol* **2020,** *457* (2), 181-190.
33. van Leeuwen, L. M.; Evans, R. J.; Jim, K. K.; Verboom, T.; Fang, X.; Bojarczuk, A.; Malicki, J.; Johnston, S. A.; van der Sar, A. M., A transgenic zebrafish model for the in vivo study of the blood and choroid plexus brain barriers using claudin 5. *Biol Open* **2018,** *7* (2).
34. Ulrich, F.; Ma, L. H.; Baker, R. G.; Torres-Vazquez, J., Neurovascular development in the embryonic zebrafish hindbrain. *Dev Biol* **2011,** *357* (1), 134-151.
35. Zhang, J.; Liss, M.; Wolburg, H.; Blasig, I. E.; Abdelilah-Seyfried, S., Involvement of claudins in zebrafish brain ventricle morphogenesis. *Ann N Y Acad Sci* **2012,** *1257*, 193-198.
36. Zhang, J.; Piontek, J.; Wolburg, H.; Piehl, C.; Liss, M.; Otten, C.; Christ, A.; Willnow, T. E.; Blasig, I. E.; Abdelilah-Seyfried, S., Establishment of a neuroepithelial barrier by Claudin5a is essential for zebrafish brain ventricular lumen expansion. *Proc Natl Acad Sci U S A* **2010,** *107* (4), 1425-1430.
37. Ando, K.; Fukuhara, S.; Izumi, N.; Nakajima, H.; Fukui, H.; Kelsh, R. N.; Mochizuki, N., Clarification of mural cell coverage of vascular endothelial cells by live imaging of zebrafish. *Development* **2016,** *143* (8), 1328-1339.
38. Lyons, D. A.; Talbot, W. S., Glial cell development and function in zebrafish. *Cold Spring Harb Perspect Biol* **2014,** *7* (2), a020586.
39. Umans, R. A.; Henson, H. E.; Mu, F.; Parupalli, C.; Ju, B.; Peters, J. L.; Lanham, K. A.; Plavicki, J. S.; Taylor, M. R., CNS angiogenesis and barriergenesis occur simultaneously. *Dev Biol* **2017,** *425* (2), 101-108.
40. O'Brown, N. M.; Megason, S. G.; Gu, C., Suppression of transcytosis regulates zebrafish blood-brain barrier function. *Elife* **2019,** *8*.
41. Isogai, S.; Horiguchi, M.; Weinstein, B. M., The vascular anatomy of the developing zebrafish: an atlas of embryonic and early larval development. *Dev Biol* **2001,** *230* (2), 278-301.

42. Moradi, M.-A.; Bomans, P. H. H.; Jackson, A. W.; van Herk, A. M.; Heuts, J. P. A., A quantitative cryoTEM study on crosslinked nanocapsule morphology in RAFT-based vesicle polymerization. *European Polymer Journal* **2018,** *108*, 329-336.
43. Moradi, M. A.; Tempelaar, S.; van Herk, A. M.; Heuts, J. P. A., Morphology Control of Liposome - RAFT Oligomer Precursors to Complex Polymer Nanostructures. *Macromolecules* **2019,** *52* (24), 9476-9483.
44. De Boeck, H.; Zidovetzki, R., Effects of diacylglycerols on the structure of phosphatidylcholine bilayers: a 2H and 31P NMR study. *Biochemistry* **1989,** *28* (18), 7439-7446.
45. Goldberg, E. M.; Lester, D. S.; Borchardt, D. B.; Zidovetzki, R., Effects of diacylglycerols and Ca2+ on structure of phosphatidylcholine/phosphatidylserine bilayers. *Biophys J* **1994,** *66* (2 Pt 1), 382-393.
46. Jimenez-Monreal, A. M.; Villalain, J.; Aranda, F. J.; Gomez-Fernandez, J. C., The phase behavior of aqueous dispersions of unsaturated mixtures of diacylglycerols and phospholipids. *Biochim Biophys Acta* **1998,** *1373* (1), 209-219.
47. Goni, F. M.; Alonso, A., Structure and functional properties of diacylglycerols in membranes. *Prog Lipid Res* **1999,** *38* (1), 1-48.
48. Szule, J. A.; Fuller, N. L.; Rand, R. P., The effects of acyl chain length and saturation of diacylglycerols and phosphatidylcholines on membrane monolayer curvature. *Biophys J* **2002,** *83* (2), 977-984.
49. Campomanes, P.; Zoni, V.; Vanni, S., Local accumulation of diacylglycerol alters membrane properties nonlinearly due to its transbilayer activity. *Communications Chemistry* **2019,** *2* (1), 72.
50. Otis, J. P.; Zeituni, E. M.; Thierer, J. H.; Anderson, J. L.; Brown, A. C.; Boehm, E. D.; Cerchione, D. M.; Ceasrine, A. M.; Avraham-Davidi, I.; Tempelhof, H.; Yaniv, K.; Farber, S. A., Zebrafish as a model for apolipoprotein biology: comprehensive expression analysis and a role for ApoA-IV in regulating food intake. *Dis Model Mech* **2015,** *8* (3), 295-309.
51. Miyares, R. L.; de Rezende, V. B.; Farber, S. A., Zebrafish yolk lipid processing: a tractable tool for the study of vertebrate lipid transport and metabolism. *Dis Model Mech* **2014,** *7* (7), 915-927.
52. Kim, J. Y.; Seo, J.; Cho, K. H., Aspartame-fed zebrafish exhibit acute deaths with swimming defects and saccharin-fed zebrafish have elevation of cholesteryl ester transfer protein activity in hypercholesterolemia. *Food Chem Toxicol* **2011,** *49* (11), 2899-2905.
53. Song, Y.; Cone, R. D., Creation of a genetic model of obesity in a teleost. *FASEB J* **2007,** *21* (9), 2042-2049.
54. Nishio, S.; Gibert, Y.; Bernard, L.; Brunet, F.; Triqueneaux, G.; Laudet, V., Adiponectin and adiponectin receptor genes are coexpressed during zebrafish embryogenesis and regulated by food deprivation. *Dev Dyn* **2008,** *237* (6), 1682-1690.
55. Anderson, J. L.; Carten, J. D.; Farber, S. A., Zebrafish lipid metabolism: from mediating early patterning to the metabolism of dietary fat and cholesterol. *Methods Cell Biol* **2011,** *101*, 111-141.
56. Liu, C.; Gates, K. P.; Fang, L.; Amar, M. J.; Schneider, D. A.; Geng, H.; Huang, W.; Kim, J.; Pattison, J.; Zhang, J.; Witztum, J. L.; Remaley, A. T.; Dong, P. D.; Miller, Y. I., Apoc2 loss-of-function zebrafish mutant as a genetic model of hyperlipidemia. *Dis Model Mech* **2015,** *8* (8), 989-998.
57. Pattipeiluhu, R.; Crielaard, S.; Klein-Schiphorst, I.; Florea, B. I.; Kros, A.; Campbell, F., Unbiased Identification of the Liposome Protein Corona using Photoaffinity-based Chemoproteomics. *ACS Central Science* **2020,** *6* (4), 535-545.
58. Muller, D. P.; Gamlen, T. R., The activity of hepatic lipase and lipoprotein lipase in glycogen storage disease: evidence for a circulating inhibitor of postheparin lipolytic activity. *Pediatr Res* **1984,** *18* (9), 881-885.
59. Ori, A.; Wilkinson, M. C.; Fernig, D. G., A systems biology approach for the investigation of the heparin/heparan sulfate interactome. *J Biol Chem* **2011,** *286* (22), 19892-19904.
60. Sun, S.; Dean, R.; Jia, Q.; Zenova, A.; Zhong, J.; Grayson, C.; Xie, C.; Lindgren, A.; Samra, P.; Sojo, L.; van Heek, M.; Lin, L.; Percival, D.; Fu, J. M.; Winther, M. D.; Zhang, Z., Discovery of XEN445: a potent and selective endothelial lipase inhibitor raises plasma HDL-cholesterol concentration in mice. *Bioorg Med Chem* **2013,** *21* (24), 7724-7734.
61. Lo, P. K.; Yao, Y.; Zhou, Q., Inhibition of LIPG phospholipase activity suppresses tumor formation of human basal-like triple-negative breast cancer. *Sci Rep* **2020,** *10* (1), 8911.
62. Thisse, B., Thisse, C. , Fast release clones: A high throughput expression analysis. Submission, Z. D. D., Ed. http://zfin.org, 2004.

63. Zhu, G.; Mock, J. N.; Aljuffali, I.; Cummings, B. S.; Arnold, R. D., Secretory phospholipase A(2) responsive liposomes. *J Pharm Sci* **2011,** *100* (8), 3146-3159.
64. Sharipov, M.; Tawfik, S. M.; Gerelkhuu, Z.; Huy, B. T.; Lee, Y. I., Phospholipase A2-Responsive Phosphate Micelle-Loaded UCNPs for Bioimaging of Prostate Cancer Cells. *Sci Rep* **2017,** *7* (1), 16073.
65. Gomez-Fernandez, J. C.; Corbalan-Garcia, S., Diacylglycerols, multivalent membrane modulators. *Chem Phys Lipids* **2007,** *148* (1), 1-25.
66. Alwarawrah, M.; Dai, J.; Huang, J., Modification of Lipid Bilayer Structure by Diacylglycerol: A Comparative Study of Diacylglycerol and Cholesterol. *J Chem Theory Comput* **2012,** *8* (2), 749-758.
67. Lindegaard, M. L.; Nielsen, J. E.; Hannibal, J.; Nielsen, L. B., Expression of the endothelial lipase gene in murine embryos and reproductive organs. *J Lipid Res* **2005,** *46* (3), 439-444.
68. Lindegaard, M. L.; Olivecrona, G.; Christoffersen, C.; Kratky, D.; Hannibal, J.; Petersen, B. L.; Zechner, R.; Damm, P.; Nielsen, L. B., Endothelial and lipoprotein lipases in human and mouse placenta. *J Lipid Res* **2005,** *46* (11), 2339-2346.
69. Ishida, T.; Choi, S. Y.; Kundu, R. K.; Spin, J.; Yamashita, T.; Hirata, K.; Kojima, Y.; Yokoyama, M.; Cooper, A. D.; Quertermous, T., Endothelial lipase modulates susceptibility to atherosclerosis in apolipoprotein-E-deficient mice. *J Biol Chem* **2004,** *279* (43), 45085-45092.
70. Badellino, K. O.; Wolfe, M. L.; Reilly, M. P.; Rader, D. J., Endothelial lipase is increased in vivo by inflammation in humans. *Circulation* **2008,** *117* (5), 678-685.
71. Lo, P. K.; Yao, Y.; Lee, J. S.; Zhang, Y.; Huang, W.; Kane, M. A.; Zhou, Q., LIPG signaling promotes tumor initiation and metastasis of human basal-like triple-negative breast cancer. *Elife* **2018,** *7*.
72. Dong, X.; Wang, G.; Zhang, G.; Ni, Z.; Suo, J.; Cui, J.; Cui, A.; Yang, Q.; Xu, Y.; Li, F., The endothelial lipase protein is promising urinary biomarker for diagnosis of gastric cancer. *Diagn Pathol* **2013,** *8*, 45.
73. Nielsen, J. E.; Lindegaard, M. L.; Friis-Hansen, L.; Almstrup, K.; Leffers, H.; Nielsen, L. B.; Rajpert-De Meyts, E., Lipoprotein lipase and endothelial lipase in human testis and in germ cell neoplasms. *Int J Androl* **2010,** *33* (1), e207-215.
74. Tatematsu, S.; Francis, S. A.; Natarajan, P.; Rader, D. J.; Saghatelian, A.; Brown, J. D.; Michel, T.; Plutzky, J., Endothelial lipase is a critical determinant of high-density lipoprotein-stimulated sphingosine 1-phosphate-dependent signaling in vascular endothelium. *Arterioscler Thromb Vasc Biol* **2013,** *33* (8), 1788-1794.
75. Sieber, S.; Grossen, P.; Bussmann, J.; Campbell, F.; Kros, A.; Witzigmann, D.; Huwyler, J., Zebrafish as a preclinical in vivo screening model for nanomedicines. *Adv Drug Deliv Rev* **2019,** *151-152*, 152-168.
76. Kemmer, G. C.; Bogh, S. A.; Urban, M.; Palmgren, M. G.; Vosch, T.; Schiller, J.; Gunther Pomorski, T., Lipid-conjugated fluorescent pH sensors for monitoring pH changes in reconstituted membrane systems. *Analyst* **2015,** *140* (18), 6313-6320.
77. Kremer, J. R.; Mastronarde, D. N.; McIntosh, J. R., Computer visualization of three-dimensional image data using IMOD. *J Struct Biol* **1996,** *116* (1), 71-76.
78. Jin, S. W.; Beis, D.; Mitchell, T.; Chen, J. N.; Stainier, D. Y., Cellular and molecular analyses of vascular tube and lumen formation in zebrafish. *Development* **2005,** *132* (23), 5199-5209.
79. Ellett, F.; Pase, L.; Hayman, J. W.; Andrianopoulos, A.; Lieschke, G. J., mpeg1 promoter transgenes direct macrophage-lineage expression in zebrafish. *Blood* **2011,** *117* (4), e49-56.
80. Schindelin, J.; Arganda-Carreras, I.; Frise, E.; Kaynig, V.; Longair, M.; Pietzsch, T.; Preibisch, S.; Rueden, C.; Saalfeld, S.; Schmid, B.; Tinevez, J. Y.; White, D. J.; Hartenstein, V.; Eliceiri, K.; Tomancak, P.; Cardona, A., Fiji: an open-source platform for biological-image analysis. *Nat Methods* **2012,** *9* (7), 676-682.
81. Schneider, C. A.; Rasband, W. S.; Eliceiri, K. W., NIH Image to ImageJ: 25 years of image analysis. *Nat Methods* **2012,** *9* (7), 671-675.